Deep Sea Research Part I:
Oceanographic Research Papers
JULY 2003; 50(7) : 863-887
http://dx.doi.org/10.1016/S0967-0637(03)00071-2

Upper-layer circulation in the eastern Equatorial and South Atlantic Ocean in January–March 1995

Herlé Mercier*[,a], Michel Arhan[a] and Johann R. E. Lutjeharms[b]

[a] Laboratoire de Physique des Océans, CNRS/IFREMER/UBO, IFREMER Centre de Brest, B.P. 70, 29280, Plouzané, France
[b] Department of Oceanography, University of Cape Town, Rondebosch, South Africa

*: Corresponding author : Fax : 00-33-2-98-22-44-96 E-mail address: herle.mercier@ifremer.fr (H. Mercier)

Abstract:

The upper-layer circulation in the eastern basin of the South Atlantic was studied from hydrographic and direct velocity measurements along WOCE lines A11, A13 and A14. A13 and A14 provide quasi-meridional samplings of the equatorial, subequatorial and subtropical circulation regimes. A13 was carried out along the African coast at about 600 km offshore from it, and A14 along the nominal longitude 9°W. A11 intersects the Cape Basin between 46°S in the west and 30°S in the east. Transport estimates were derived from direct velocity measurements and a box inverse model. In the equatorial eastern Atlantic, the Equatorial Undercurrent (EUC) transport decreases from 25×10^6 m^3 s^{-1} at 9°W to 13×10^6 m^3 s^{-1} at 5°E. Re-circulations of the EUC into the northern and equatorial branches of the South Equatorial Current (SEC) are evidenced at 5°E and quantified. In the tropical Atlantic, we estimate 7.5×10^6 and 4.2×10^6 m^3 s^{-1} for the transports at 9°W of the South Equatorial Undercurrent (SEUC) and South Equatorial Countercurrent (SECC), respectively. Both the SEUC and SECC extend vertically down to intermediate depths and contribute to the northern limb of the Angola Gyre. The Angola Current transport is estimated to be $16\pm5\times10^6$ m^3 s^{-1} for $\sigma_1<32.1$ at 13°S. South of the Angola Gyre, the transports show an apparent cyclonic circulation, developed mostly at the intermediate level. The water mass properties suggest that it is, at least partially, a re-circulation of the Benguela Current. Further south and for the subtropical gyre, we estimate $10\pm5\times10^6$ m^3 s^{-1} for the transport of the South Atlantic Current across 9°W and $28\pm4\times10^6$ m^3 s^{-1} for the transport of the Benguela Current at 10°E for $\sigma_1<32.1$.

Keywords: Equatorial Atlantic; South Atlantic; Circulation; Current; Hydrography

1. Introduction

Between January and March 1995, two quasi-meridional hydrographic sections were carried out in the Equatorial and South Atlantic Ocean at 9°W (A14) and parallel to the African coast at about 600 km offshore (A13), as part of the French contribution to the Hydrographic Program of the World Ocean Circulation Experiment (WOCE) (Fig. 1). The A13 meridional line was complemented with a transverse line joining its southern end to the South African Coast (Fig. 1). We will refer to this transverse line as the "Cape Town line". The large-scale circulation patterns intersected by these sections can be inferred from Stramma and England's (1999) schematics of the South Atlantic circulation at 100-500 m depth (Fig. 2). In the equatorial area, the hydrographic lines intersect the eastward jets originating at the western boundary and their re-circulations as branches of the South Equatorial Current (SEC). These eastward jets also feed the Angola Gyre, which appears on Figure 2 as a partly isolated feature limiting the eastward extent of the South Equatorial Counter Current (SECC). In this sub-equatorial region, the circulation patterns cut by A14, characterized by an alternation of zonal jets, significantly differ from that cut by A13, which is dominated by the Angola Gyre. The transition between the tropical and sub-tropical regimes is located at about 18°S in the Angola-Benguela Front (Meeuwis and Lutjeharms, 1990). This front is most intense at the sea surface (e. g. Mohrholz et al., 2001), particularly near the coast. A branch of the Angola Current, which transports tropical water to the subtropical gyre, joins the southern branch of the SEC (Fig. 2). This branch of the SEC and the Benguela Current farther southwest close the sub-tropical gyre, the southern limit of which is the South Atlantic Current, which was fully sampled by A14, but not necessarily by A13.

In this paper, we provide estimates of the transports across the hydrographic sections using a box inverse model (Mercier 1986; Lux et al. 2001). We focus on the upper-layer hydrography and circulation as revealed by these data. Another paper will discuss the deep and bottom layer hydrography and circulation. While our results will be shown to be generally compatible with those summarized by Stramma and England's (1999), some adjustments will be suggested, and a quantification of the main circulation features will be proposed. The few qualitative adjustments concern the equatorial and subequatorial domains that in the past have been the less well sampled region of the South Atlantic. Owing to the inverse approach, and

despite still significant uncertainties, the quantitative results show the advantage of being coherent in terms of property conservation over the latitudinal spread of the South Atlantic. In the eastern equatorial domain, they provide estimates of the main zonal jets for comparison with the more numerous results from the western basin. In the subtropical South Atlantic, the transport estimates will be shown to agree with those from a previous study by Gordon et al. (1992), but show differences with others (e. g. Garzoli et al., 1996).

2. The data and air-sea fluxes

The Cither 3 cruise, which was carried out from the French *N. O. L'ATALANTE* in January-March 1995, occupied 243 hydrographic stations along A14, A13, and the Cape Town line. The cruise started with the A14 leg at 9°W, which was conducted from north to south. After a call at Cape Town, the Cape Town line was conducted before A13 carried out from south to north.

We used the Cither 3 $CTDO_2$ (conductivity temperature depth dissolved-oxygen) measurements, the silicate bottle data, and the *N. O. L'ATALANTE* 75 kHz ADCP data. The data calibration procedures are described in reports by Le Groupe Cither 3 (1996 a-b). The $CTDO_2$ data accuracies are within the WOCE standard as defined by the WOCE Hydrographic Programme Office (1994) and silicate accuracy is better than 0.2 μmol kg^{-1}. The ship heading and position needed to estimate the absolute velocity from the ADCP were obtained from the ship gyrocompass and standard GPS (Global Positioning System). Errors in the estimation of the absolute velocity from the ADCP come mainly from the estimation of the ship heading and are evaluated to 0.05 m s^{-1}.

The absolute transports perpendicular to the hydrographic lines were estimated with an inverse model similar to that employed by Lux et al. (2001). The model is based on mass and property (heat, salt, and silicate) conservations in closed boxes delimited by the hydrographic lines and the coast. In order to construct a closed box including A14, we added to the Cither-3 data the eastern part of the A11 line carried out in January 1993 by Saunders and King (1995; Fig. 1). We note that A11 and A14 were both carried out during the same month but at two

years apart. Two closed boxes are thus defined: Box I delimited by A14, A11 and the African coast, and Box II delimited by A13, the Cape Town line and the African coast (Fig. 1). The intersection between A14 and A11 occurs at 41° 30'S and 9°W.

In addition to the Cither-3 and A11 data, and for comparison purposes, we also occasionally refer to data from the AJAX section realized in 1983 along the Greenwich meridian (Whitworth and Nowlin, 1987; Fig.1).

The air-sea fluxes integrated over the top areas of the boxes and the Ekman transports across their lateral boundaries are needed to write the conservation equations of the inverse model. The Ekman transports perpendicular to the hydrographic lines and their variability were estimated from the ECMWF (European Centre for Medium-Range Weather Forecast) model outputs averaged for the three months of the Cither 3 cruise (January-March 1995). The Ekman transport integrated along Box I (Box II) is equal to $-0.7 \pm 0.7 \times 10^6$ m^3 s^{-1} ($-4.6 \pm 1.2 \times 10^6$ m^3 s^{-1}), with positive (negative) values indicating flows into (out of) the box. The Ekman transports between 3°N and 3°S were not taken into account because of the breakdown of the Ekman theory close to the equator. Between 20° and 35°S, the northward wind stress component is intensified close to the African coast compared to further west, hence the difference in Ekman transport between Box I and Box II. At the African coast, the seaward Ekman transport drives the Benguela upwelling. The ECMWF air-sea heat fluxes averaged for January-March 1995 are directed from the atmosphere to the ocean and estimated to be $0.4 \pm 0.2 \times 10^{15}$ W for Box I and $0.1 \pm 0.15 \times 10^{15}$ W for Box II.

3. Water masses and dynamical regimes

The inverse model requires that layers be defined for which mass and tracer conservations are imposed. The layers were chosen to correspond roughly to the major water masses in the eastern South Atlantic (Table 1). The dynamical regimes intersected by the hydrographic lines are discussed in this section in the light of the vertical distributions of properties (potential temperature, salinity, dissolved oxygen) along A14, A13 and the Cape Town line (Figs. 3 to 5), as well as from plots of salinity and oxygen on $\sigma_0 = 26.3$ and $\sigma_1 = 31.85$ in the central and

intermediate waters, respectively (Fig. 6). This analysis will be useful for the setting-up of the inverse model as well as for the validation and interpretation of the circulation schemes.

3.1 Equatorial and subequatorial regions

In the equatorial region, the eastward Equatorial Undercurrent (EUC), South Equatorial Undercurrent (SEUC), and SECC are identified from relative maxima in salinity or oxygen (Figs. 3, 4 and 6). In particular, the lateral oxygen maximum above 200 m depth at 10°S on A13 (Fig. 4c) is associated with the SECC (see section 4). A similar pattern, yet wider (from ~4°N to ~5°S) and deeper (to 300 m), encompasses the EUC and SEUC in both lines (Figs. 3c, 4c). These currents re-circulate into the various branches of the SEC and also contribute to the Angola Gyre (Gordon and Bosley, 1991; Wacongne and Piton, 1992; Fig. 2), whose centre, located at about 13°S and 5°E, falls on A13. In Fig. 4, the Angola Gyre is recognized as a well-defined doming of the isotherms and isohalines at this latitude in the 100-400 m depth range. A salinity maximum is found on σ_0 = 26.3 at the same latitude (Gordon and Bosley 1991) not only on A13, but also on A14 and Ajax (Fig. 6). The vertical salinity distributions (Figs. 3b, 4b) reveal that these maxima at σ_0 = 26.3 are subsurface signatures of surface-intensified patterns. An examination of the large scale surface salinity distribution (e.g. Tomczak and Godfrey, 1994, their Fig. 2.5) shows that these high salinities are not related specifically to the Angola Gyre, but should be regarded as the eastern part of the basin-wide extent occupied by the Salinity Maximum Water formed by excess evaporation in the South Atlantic. The correspondence between the high salinities and the central latitude of the Angola Gyre probably results from a cyclonic entrainment of fresher equatorial water by the gyre on its eastern side (Gordon and Bosley, 1991).

The cyclonic circulation within the Angola gyre also shows a signature in the dissolved oxygen distribution (Fig. 4c). The northern limb of the gyre is characterized by a relatively high oxygen content in the Central Water to the north of 13°S, particularly north of 5°S (in the SEUC and EUC) and at 10°-13°S (the SECC). Oxidation at the African continental shelf decreases the oxygen of the central water within the southward Angola Current, and the cyclonic circulation advects this lower-oxygen water to the south of the gyre centre. On A13 this results in a front at ~13°S in the 100-300 m depth range. There is no similar clear-cut

oxygen front on A14 (Fig. 3c), yet low oxygen values observed immediately to the north of 15°S around 300 m depth suggest an origin at the eastern boundary with subsequent westward advection. The doming of the isotherms at 9°W (Fig. 3a) near 10°S at 9-10°C and near 7°S at 12-14°C marks the boundary between this westward flow (the central branch of the SEC, Fig. 2) and the generally eastward subequatorial flow. The existence of a similar pattern and of low oxygen values in the vicinity of the South American coast (Mémery et al., 2000) suggests that the cyclonic subequatorial circulation at 100 m - 300 m depth extends westward throughout the basin.

At the intermediate level, the oxygen maximum found at ~ 650 m depth near 2°S in the vertical property sections (Figs. 3 and 4) and on σ_1 = 31.85 (Fig. 6b), along with the salinity minimum at 2°S (Fig. 6a), suggests an eastward flow of relatively young Antarctic Intermediate Water (Suga and Talley, 1995). On σ_1 = 31.85, the salinity maximum and oxygen minimum centred at about 10°S on A14 and 12°S on A13 (Fig. 6) were documented by Tsuchiya et al. (1994) and Suga and Talley (1995), who ascribed their origins to intense vertical mixing and oxygen consumption at the eastern boundary. Suga and Talley (1995) suggested westward transport of intermediate water at those latitudes. South of about 14°S, intermediate water is both fresher and more oxygenated than the equatorial input, and an additional (subtropical) source is required to maintain those properties.

3.2 Subtropics

The Angola-Benguela Front, which marks the transition between the subequatorial and subtropical gyres (Meeuwis and Lutjeharms, 1990; Gordon and Bosley, 1991), appears as successive salinity fronts on σ_0 = 26.3, the largest front being centred at about 16°S on A14, Ajax, and A13 (Fig. 6a). The relative salinity maximum between 18° and 20°S along A14 might be related to meanderings of the front or to the existence of multiple fronts. The Angola-Benguela front also corresponds to a transition in oxygen (Mohrholz et al., 2001; Figs. 3 and 4). At the intermediate level, the front is located between 22°S and 24°S on A13 and at 23°S on A14 from both salinity and oxygen on σ_1 = 31.85 (Fig. 6). It is shifted southward compared to its location within the central water as suggested by Stramma and England (1999; compare their Figs. 3 and 4).

Arhan et al. (1999) pointed out the high density of the eddy population in the subtropical domain of the Cape Basin. They studied more particularly three Agulhas rings that were intersected close to their centres by A14 (near 30°S and 26°S; Fig. 3), and by the Cape Town line (11°E; Fig. 5), and discussed other structures, either anticyclonic or cyclonic, that were less well sampled. Another prominent mesoscale feature not described by those authors is the oxygen-depleted structure at 23°S on A13, and the associated oxygen maximum to its north. This is probably the signature of a mesoscale dipole generated at the Angola-Benguela Front. The salinity minimum (maximum) associated with the northern (southern) structure at the intermediate level (Fig. 4), and the isopycnal slopes within the central water, substantiate a dynamical origin for the oxygen patterns. We note, however, that Bubnov (1972) and Chapman and Shannon (1987) identified a nearby site of formation of oxygen minimum in the Walvis Bay area at 24°S that is separated from the tropical oxygen minimum by larger oxygen values between 19°S and 22°S.

The southern limit of the subtropical gyre is marked by the Subtropical Front (STF), which is associated with the South Atlantic Current (Stramma and Peterson, 1990). The STF is intersected at 37°S by A14 (Figs. 3 and 6), at 38°S by A13 (Figs. 3 and 6) and at 12°E by the Cape Town line (Fig. 5). Smythe-Wright et al. (1998) located the STF in the band 3°W-5°E on A11. Therefore, and for further use, we note that the segments of both A14 and A11 that contribute to Box I fully intersected the South Atlantic Current. In contrast, the Subantarctic Front (SAF) was intersected by both A11 and A14 outside of the perimeter of Box I.

The northern and southern limbs of the subtropical gyre, formed respectively by the Benguela and South Atlantic Currents, present contrasting values in oxygen because the Benguela Current is carrying relatively low-oxygen water from the Indian Ocean mixed with South Atlantic Current water (Gordon et al., 1992). On both meridional sections, the South Atlantic and Benguela Currents, which are found on each side of the subtropical bowl, are associated with oxygen values respectively higher and lower than about 220 μmol kg^{-1} in the central water (Figs. 3 and 4). Looking at the Cape Town line (Fig. 5), the core of the Benguela Current transport is associated with the upward sloping isotherms and isohalines between 16°30'E and the continental slope and is characterized by a relative minimum in oxygen (< 210 μmol kg^{-1}) at the central and intermediate water levels. Gordon et al. (1992) argue that

this oxygen minimum traces Indian Ocean Water. Both oxidation within the Benguela upwelling regime, and tropical water input from the north, contribute to the maintenance of this oxygen minimum further downstream (Figs. 3 and 4). At the intermediate water level the oxygen minimum is associated with salinity values higher than 34.35 (thus higher than those found in the South Atlantic Current) indicating a significant Indian Ocean contribution (Fig. 5).

Gordon et al. (1995) showed that tropical water is transported by a poleward undercurrent along the African continental slope at about 250 m depth, at least up to 27°S (see also Shannon and Nelson, 1996). This undercurrent, however, does not seem to be present permanently (Mohrholz et al., 2001). A similar poleward undercurrent can be identified around 200 m depth on the Cape Town line from the splitting of the isotherms and isohalines at the approach of the African continental shelf break, which indicates a velocity core at a depth of 300 m (Fig. 5). This core is associated with oxygen depleted water and southward velocities as revealed by ADCP measurements (not shown). Contrary to what was observed at 27°S by Gordon et al. (1995), an analysis of the θ–S characteristics in the core of the poleward undercurrent on the Cape Town line reveals a subtropical origin of the water (not shown). Thus, the oxygen minimum observed at 34°30'S at the continental shelf break is most likely associated with local consumption and does not denote a tropical origin.

4. Direct transport estimates in the tropics

The zonal velocity measurements from the vessel-mounted ADCP along A14 and A13 present new information on the sub-surface circulation in a region where such measurements are few (Fig. 7). The ADCP velocity section at 9°W shows many similarities, north of 4°S, with those at 35°W (e. g. Stramma and Schott, 1996), allowing us to identify the intersected currents by assuming zonal coherence. At 9°W, the sub-surface eastward currents include the EUC at the equator and the SEUC at 4°S. The westward currents observed below the EUC, to the north and south of its core, are the northern and equatorial branches of the South Equatorial Current (NSEC and ESEC). The shallowness of the EUC at such longitudes and the upward limitation of the current measurements at 28 m depth prevent us from detecting any surface current. On the salinity section (Fig. 3), however, the presence of fresher water above the more saline

EUC reveals a thin layer of westward surface flow. The weak eastward sub-surface current at 2°30'N might be the signature of the NEUC (the northern counterpart of the SEUC), although this current is expected mainly to feed the Guinea Dome (Voituriez, 1981). At the intermediate levels, the eastward currents below about 400 m with cores at 2°S and 1°30'N are the northern and southern Intermediate Counter Currents (NICC and SICC).

The transports of 24.6 x 10^6 m^3 s^{-1} and 7.5 x 10^6 m^3 s^{-1} that we respectively estimate for the EUC and SEUC at 9°W (Table 2) are similar to mean values quoted at 35°W and 30°W by Stramma and Schott (1999) and Bourlès et al. (1999). Stramma and Schott (1999), using velocity measurements by Bubnov and Egorikhin (1980), reported 36.4 x 10^6 m^3 s^{-1} and 20.5 x 10^6 m^3 s^{-1} for the averaged transports for the EUC and SEUC at 23°W in June-September 1974, which is larger than the estimates at 35°W and 9°W. Also, Molinari (1982) quoted highly variable geostrophic transport estimates in the range 5 to 23 x 10^6 m^3 s^{-1} for the SEUC between 25° and 28°W. Because of the time-variability, the agreement between our snapshot transport estimates at 9°W and the mean transports reported at 35°W by Stramma and Schott (1999) is likely coincidental.

At 9°W (A14) a weak surface signature of the SECC is found at 11°S (Fig. 7a), but the more intense sub-surface signal associated with that current is centred at 9°S. It extends to the intermediate water level. We estimate 4.2 x 10^6 m^3 s^{-1} for the transport of the SECC in the upper 300 m (Table 2) which is comparable to values found in the western basin: Molinari (1982) reported 3 to 7 x 10^6 m^3 s^{-1} for the transport of the SECC at 25°-28°W; Wienders et al. (2000) estimated 5 x 10^6 m^3 s^{-1} for the transport of the SECC at about 30°W (see also Reverdin et al. 1991). The NSEC and ESEC transports are about 5 x 10^6 m^3 s^{-1} each (Table 2).

Along A13, which samples the equatorial region between 0° and 5°E longitude, eastward currents with velocity cores above 100 m are found at 4°N, the equator, 4° 30'S, and south of 9°S (Fig. 7b). The eastward current at 4°N is the signature of the Guinea Current, which forms the northern limb of an anti-cyclonic circulation cell in the northern Guinea Basin (Hisard, 1975). The westward extension of the Guinea Current varies seasonally and is limited to about 9°W in boreal winter (Hisard, 1975), which might explain why this current was not observed at 9°W in January 1995 (Fig. 7a). The transport of the EUC decreases from

24.6 x 10^6 m^3 s^{-1} at 7°W (A14) to 12.6 x 10^6 m^3 s^{-1} at 2°E (A13) (Table 2). The ADCP measurements along A13 reveal westward currents on both sides of the EUC that are associated with salinity maxima (Fig. 4), which strongly suggests that they are recirculations of the EUC. Those westward currents are the NSEC and ESEC shown in the schematics of Stramma and England (Fig. 2), which altogether carry 14.8 x 10^6 m^3 s^{-1} for the same depth range as that of the EUC (Table 2).

The termination of the EUC was studied with the salinity maximum at the core of the EUC as a tracer (Wacongne and Piton, 1992). At the eastern boundary, the EUC bifurcates into northward and southward currents along the Biafra Bight and Gabon-Congo Bight, respectively. In the A13 ADCP measurements, the sum of the transports of the eastward Guinea Current and EUC balances that of the westward NSEC and ESEC in the first 190 m (Table 2) indicating that the contribution of the Guinea Current and EUC to a southward eastern boundary current (the Gabon-Congo Current; Wacongne and Piton, 1992) might be weak (about 1 x 10^6 m^3 s^{-1}).

At 9°W, the equatorial thermostad (Tsuchiya, 1986) is characterized by a stratification minimum at potential temperatures 13°C-15°C (Fig. 3). The southward extension of the equatorial thermostad is limited to 4°30'S at the very location of the SEUC that actually forms the southern boundary for this water mass. Along A13, the equatorial thermostad is associated with higher potential temperatures (14°-17°C) than at 9°W and extends southward to 8°30'S (Fig. 4). This agrees with Tschuchiya's (1986) analysis revealing a poleward bending for the southern limit of the thermostad east of 0°W and with the analysis of the density field along a WOCE line at 4°30'S (Arhan et al., 1998) that suggests a southward geostrophic flow within the equatorial thermostad around 0°W. Between about 5°S and 18°S, A13 intersects the Angola Gyre (Fig. 2), and the eastward current observed at 4°45'S appears as the northern limit of this gyre (Fig. 7b). We note that this current extends from the upper limit of the ADCP measurements at 28 m down through the thermocline to about 300 m with a core found within the main thermocline, and not below the thermocline as for the SEUC at 9°W. As suggested by previous studies (Fig. 2; Stramma and England, 1999; Gordon and Bosley, 1991), this current is the superimposition of the SEUC with the surface-intensified flow of the Angola Gyre. The weaker eastward flow between 8°30' and 12°30'S also

contributes to the Angola Gyre northern limb. The oxygen maximum at 10°S between 100 m and 200 m (Fig. 4) suggests a contribution of the SECC to this flow. The eastward transport in that latter region is equal to 8 x 10^6 m^3 s^{-1}. Finally, we note that the NEUC is not observed on A13.

The SICC (South Intermediate Countercurrent) appears at 1°S-2°30'S along A13 as a maximum eastward velocity at depths 600 – 800 m (Fig. 7b), deeper than at 9°W (~500 m; Fig. 7a). The signatures of the NICC and EIC (North Intermediate Countercurrent and Equatorial Intermediate Current) are weak. A few LADCP (Lowered Acoustic Doppler Current Profiler) profiles available within the SICC allow us to estimate a transport of 9 ± 5 x 10^6 m^3 s^{-1} for the depth range 400 - 1000 m (the estimated error on the LADCP transport was based on a assumed 0.05 m s^{-1} bias in the data). This is comparable to the 11.2 x 10^6 m^3 s^{-1} found at 35°W by Stramma and Schott (1996), for instance.

5. The inverse model

The box inverse model is similar to that used in Lux et al. (2001) and Wienders et al. (2000). The reader should refer to these papers for a detailed description of the model and to Wunsch (1996) for a review of box inverse modelling in oceanography. In this section, we briefly summarize the model settings and discuss the sensitivity of the circulation estimates to a priori choices for the inverse model. The model will be applied to box I (defined by A14 and A11) and box II (defined by A13 and the Cape Town line) independently in order to prevent excessive bias due to time variability especially in the tropics where the equatorial currents were sampled at a three-month interval by the two meridional lines. We note that, although the circulations in the two boxes are estimated independently, the results of the two inversions show good agreement. Before building box I from the two non-synoptic lines A14 and the eastern part of A11, we verified that the water masses were similar at their crossing point and that both lines fully intersected the South Atlantic Current (see section 3.2). No major incompatibility was found between A14 and A11, nor in the results of the inverse model using these two lines (Box I, see below).

5.1 The unknowns

The unknowns of the inverse model are :

1. The reference level velocity U_r, normal to the hydrographic lines, for all station pairs located at off-equatorial latitudes ($|\text{Lat}| \geq 3°$).
2. The transports T_{eq} for each water mass defined in Table 1 for each station pair in the equatorial band ($|\text{Lat}| < 3°$).
3. The vertical diffusitivies K_v at the interface between two layers. The layer limits are the same as those used for defining the water masses (Table 1).

The model looks for best estimates of these unknowns by minimizing, in a least-squares sense, the weighted sum of the squared departures of the unknowns from a priori values and the squared residuals of the constraints (Mercier 1986; Tarantola and Valette 1982). The weights are error covariance matrices. At off-equatorial latitudes, the thermal-wind equation and the knowledge of U_r allow us to compute the absolute velocity profiles between station pairs. In the equatorial band, the water mass transports between station pairs are directly estimated by the model (the T_{eq}). The vertical diffusivities K_v are used to compute the diffusive fluxes in the tracer constraints that are written as a balance between 3D-advection and vertical diffusion. It is assumed that the K_v are the same for all tracers.

5.2 The reference levels and the a priori values of the unknowns

The a priori circulation depends on the reference level chosen for the integration of the thermal-wind relationship. We summarize below the choices of the reference levels that are based on tracer inferences. The transports resulting from those choices are presented in Figs. 8 and 9.

Box I (A14-A11): North of 3°N the reference level is chosen at the bottom, lacking a better choice. From 3°S to 13°S, an oxygen minimum in the deep water (not shown) suggests a westward mean flow from the eastern boundary that we obtain by choosing the reference level at 2000 m above the oxygen minimum. As discussed below, this choice will prove problematic between 8°S and 10°S and will need modification in this latitude range. From 13°S to 23°S, the oxygen field presents a maximum in the deep water related to an eastward

flow (see Speer et al., 1995) that is obtained by setting the reference level at the bottom. Note that using a reference level above the deep water, as suggested by Speer et al. (1995), would result in much larger transports for the lower part of the deep water in the Angola basin (not shown) than those reported by Warren and Speer (1991). South of 23°S and along A11, the reference level is chosen at the interface between the upper circumpolar water and the deep water of northern origin (σ_1 = 32.28). Off the African shelf, particularly, this choice results in a northward transport of central and intermediate waters within the Benguela Current and southward transport of deep water.

Box II (A13 and Cape Town line) : North of 3°N, the thermal-wind relationship leads to horizontal velocities of several m s^{-1}, probably due to an energetic wave field close to the African continental slope. Thus, between 3°N and the African coast, we decided to solve for the water mass transports between station pairs (T_{eq}) as in the equatorial band. From 3°S to 13°S, a large vertical shear of the geostrophic velocity within the lower deep water led us to choose the reference level at 3300 m within this water mass to prevent too large a priori transports. From 13°S to 23°S, a bottom reference level is chosen for the same reasons as for Box I. South of 23°S, in the Cape Basin, the reference level is chosen at the interface between the upper circumpolar water and the deep water as for Box I.

The method requires setting a priori values and error covariance matrices for the unknowns. The reference level velocities U_r are initialised to zero with an error standard deviation of 0.01 m s^{-1} except close to the continental slopes, where a standard deviation of 0.1 m s^{-1} is taken. The a priori values of the equatorial transports T_{eq} are set to zero with standard deviations of 3 x 10^6 m^3 s^{-1} for the SW and TW layers, 2 x 10^6 m^3 s^{-1} for the IW, UCW, DW, LDW and 1 x 10^6 m^3 s^{-1} for the BW (layer abbreviations are defined in Table 1). Vertical diffusivities K_v are set to 1 x 10^{-4} m^2 s^{-1} for the layers above the DW and 5 x 10^{-4} m^2 s^{-1} for the DW and BW layers to take into account a likely increase of Kv with depth (Polzin et al., 1997). The standard deviations are used to build the error covariance matrix associated with the a priori choice. This matrix is assumed diagonal (no error correlation).

5.3 The constraints

The constraints of the inverse model and the associated errors are defined in Tables 3 and 4. They include mass, heat, salt, and silica conservations in Boxes I and II as well as transport specifications from ADCP measurements for the equatorial and sub-equatorial currents identified in Section 4. A transport constraint derived from Lux et al. (2001) is added to control the lower deep water transport across A14 north of 4°30'S (Table 3). The errors associated with the constraints were estimated along the lines defined by Lux et al. (2001), as summarized below (see also Ganachaud, submitted). For the mass, heat, salt and silica conservations in layers that are not in contact with the atmosphere, the uncertainties are taken equal to the a priori diffusive transports at the top of the layer. For the vertically integrated mass and tracer conservations, errors include the error contribution of air-sea fluxes (Ekman transports and, when relevant, air-sea heat flux) estimated as the standard deviation of ECMWF data for the three months of the cruise (see Section 3), errors linked to the neglect of the river inputs and transports on continental shelves (estimated to be 2 x 10^6 m^3 s^{-1}) and errors in bottom triangles (estimated to be 1 x 10^6 m^3 s^{-1}). For transport estimated from ADCP measurements, we assumed a bias error of 0.05 m s^{-1} in the measured velocities.

5.4 The reference solution

The inverse model runs using the above choices revealed for Box I (A14-A11) inconsistencies between some of the upper layer ADCP transports used to constraint the model (Table 3) and the a posteriori circulation. The largest inconsistencies occured in the latitude range 8°-10°S, where we had to increase the standard deviation of the reference level velocity from 0.01 m s^{-1} to 0.05 m s^{-1}. This change resulted in a deep cyclonic circulation in the Angola Basin, in agreement with Warren and Speer, 1991. It was verified that after inversion the residuals of the constraints and the deviations from the a priori solution were all consistent with the a priori error covariance matrices. The accumulated transports in the upper layer (surface to σ_1=32.1) resulting from these settings are presented and compared to the a priori solutions in Figs. 8 and 9. They are referred to in the following as solution S1. The error bars shown in the same figures result from the least-squares formalism. The differences between the a priori and a posteriori solutions will be discussed latter.

5.5 Sensitivity of the a posteriori circulation to a priori choices

Several experiments were conducted to determine the sensitivity of the solution to a priori choices of the reference levels, to errors in the unknowns and in the constraints, and to adding addition of information on the circulation (Figs. 8 and 9).

- *Sensitivity to the choices of the reference levels and a priori errors on the reference level velocities.* Having noted that our setting of the reference level at $\sigma_1 = 32.28$ along A11 in experiment S1 differs from that of Saunders and King (1995) who selected a reference level at $\sigma_4 = 45.96$, we ran the inverse model with reference levels along A11 and the Cape Town line set at $\sigma_4 = 45.96$ (experiment S3). Also, in an independent run, the errors on the reference level velocities were multiplied by 2 at all station pairs (experiment S6). The modifications in the solutions are small. S3 and S6 show only local departures from the reference solution S1.

- *Sensitivity to the a priori values of the reference level velocities*. Three attempts are reported here. First, three Agulhas rings were intersected by A14 and the Cape Town line (Section 3), which were described by Arhan et al. (1999). They used the ADCP measurements at 250 m to estimate the absolute geostrophic velocity profiles within the rings. In experiment S5, we similarly set the reference level to 250 m within the Agulhas rings, with the reference level velocities constrained to the observed ADCP velocities with an error bar of 0.05 m s^{-1}. The second attempt was motivated by the observation that the transport associated with the subtropical front in experiment S1 (about 10 x 10^6 m^3 s^{-1}) is less than previous estimates that often are in the range 20 to 30 x 10^6 m^3 s^{-1} (e.g. Smythe-Wright et al. 1998). The Lagrangian float measurements at 800 db reported by Boebel et al. (1999) reveal average velocities of about 0.05 m s^{-1} in the STF, somewhat larger than those diagnosed by the inverse model in experiment S1. In S2 we add this information in a 2° latitude band centred on the STF on A14, setting there the reference level at 800 db with an a priori velocity value of 0.05 ± 0.02 m s^{-1}. Third, we noted that Saunders and King (1995) imposed a transport of 5 ± 4 x 10^6 m^3 s^{-1} to the poleward undercurrent off the African coast on one of their solutions. This poleward undercurrent was also detected on the Cape Town line, but the ADCP measurements revealed a weaker southward transport of 0.3 ± 0.3 x 10^6 m^3 s^{-1} between

100 and 300 m east of 17°E. In experiment S4, we constrained the model to satisfy those transport estimates. First considering Box I (Fig. 8), solutions S4 and S5 differ from S1 in the equatorial region where an increase in the upper-layer eastward transport is observed to balance the additional mass flux out of Box I imposed by the constraints. In experiment S2, the transport of the SECC at 9°S decreases compared to S1, in order to balance the required increase in the South Atlantic Current eastward transport. The adjustments are smaller for Box II.

- *Sensitivity to the choices of errors in the constraints.* In experiment S7, we multiplied the a priori errors in the tracer conservation constraints by a factor of 2. The changes of circulation are within the a posteriori error bars for S1 (Figs. 8 and 9). We also verified that the a posteriori circulation is only weakly sensitive to the a priori settings of the vertical diffusivities (not shown). This result obtained in a region where mid-latitude dynamics prevail is at variance with the results of Lux et al. (2001), who found in the equatorial region that the a posteriori circulation from a similar box inverse model was sensitive to the amplitude of the vertical diffusive fluxes of deep water.

- *Sensitivity to the wind forcing.* In experiments S1 to S7, the wind stress is an average for January-March 1995 as our goal is to estimate the circulation for the months of the cruise. At variance with this approach, some global inverse modelling studies (e. g. Ganachaud, 1999) look for an annual average of the circulation. To estimate the differences between the two approaches, we ran experiment S8 in which the wind stress is the annual average for 1995. Departures from our reference solution S1 are local and the differences between S8 and S1 are smaller than the error associated with S1 (Figs. 8 and 9).

In summary, these sensitivity studies show that reasonable changes in the model settings result in mostly local modifications of the solutions that are within the error bars of the reference solution S1. Experiment S4 (box I) is an exception which suggests that the constraint on the transport of the poleward current was not realistic. Therefore, we will focus

our discussion on S1, keeping in mind that the range of acceptable solutions is described by the associated uncertainties.

6. The circulation

6.1 The equatorial and sub-equatorial domains

The equatorial and sub-equatorial regions are characterized by a net eastward transport in the upper-layers that reaches a maximum at about 13°S (Figs. 8, 9). At 9°W (A14), the net eastward transport results from the contributions of the EUC, SEUC, and SECC, which are separated by westward transports associated with the equatorial and central branches of the SEC (Fig. 8; Fig. 2). Closer to the eastern boundary (Fig. 9; A13), the larger contributions to the net eastward flux come from the EUC and the northern limb of the Angola Gyre. Maximum cumulative eastward transports of $11.8 \pm 5.0 \times 10^6$ m^3 s^{-1} (across A14) and $16.5 \pm 5.0 \times 10^6$ m^3 s^{-1} (across A13) are reached at 13°S across A14 and A13, the latitude of the Angola Gyre centre as determined from the salinity field (Fig. 6).

At the intermediate level, the SICC is best identified across A13 (Fig. 10). The SICC is found immediately south of the equator with a transport of about 3×10^6 m^3 s^{-1}, somewhat less than the transport estimated from the LADCP data. Note the correlation between the central water and intermediate water transports, especially at 9°W across A14 at the locations of the SEUC and SECC, in agreement with the ADCP measurements.

Gordon and Bosley (1991) estimated 5×10^6 m^3 s^{-1} for the Angola gyre transport in the 0-300 db layer between 5°S and the gyre center. This estimate compares well with our estimate of 6×10^6 m^3 s^{-1} for the transport of the surface and central water layers (0-400 m) in the same latitude band at 5°E (Fig. 10). The inverse model locates the bulk of the transport of the Angola Gyre in the surface and central water layers. This agrees with Gordon and Bosley's findings about the surface intensification of the gyre, as with the gyre tracer signatures that are most pronounced above 300 m depth (section 3). On Fig. 9, the prominent peak of the cumulative transport curve between 10°S and 15°S should be associated with the core of the Angola Gyre as described by Gordon and Bosley (1991). However, the observation of current

reversals at 13°S on both meridional lines (Figs. 8, 9) corroborates the inference drawn from the salinity and oxygen patterns (Figs. 3, 4, 6) that this feature is embedded in a cyclonic gyre extending westward to at least the Mid-Atlantic Ridge, and probably the South American continental slope.

Because of the volume conservation and assuming negligible diapycnal flow, the transport of the Angola Current at a given latitude balances the cumulative eastward transport along A13 at that latitude. Considering the surface and thermocline water layers, the Angola Current transport is 11 x 10^6 m^3 s^{-1}, thus 5 x 10^6 m^3 s^{-1} larger than the eastward transport between 5°S and 13°S at 5°E (Fig. 10). Gordon and Bosley (1991) found that the eastward transport associated with the Angola Gyre between 5°S and 13°S at 5°E was similar to that estimated east of 5°E at 13°S. Our different result suggests that some of the southward transport in the eastern limb of the Angola Gyre takes place in an eastern boundary current along the coast of Africa that was missed by the data set used by Gordon and Bosley (1991). This hypothesis is supported by observations by Moroshkin et al. (1970) of an intense Angola Current covering the African shelf and continental slope between 9° and 16°S. This also implies that about half of the Angola Current transport originates north of 5°S (Fig. 9), and supports the idea of an Angola Gyre embedded in a larger scale sub-equatorial cyclonic gyre as anticipated from the tracer fields.

Although Gordon and Bosley (1991) concluded that the centre of the Angola Gyre at 500 db was shifted southward near 18°S, no southward shift of the gyre centre is apparent in the transport plots at the Antarctic Intermediate Water level (Fig. 10). Rather, there is some indication from both the A14 and A13 transport curves of an eastward flow immediately south of 15°S with an upper layer transport of about 8 x 10^6 m^3 s^{-1} across both lines (Figs. 8 and 9). This feature is best defined at the intermediate level (Fig. 10). The eastward current is associated with the large salinity decrease marking the Angola-Benguela Front on σ_0 = 26.3 across A14 and A13 (Fig. 6a). At the intermediate level, it carries relatively fresh and oxygenated water that cannot originate from the equatorial source (Fig. 6). This transport reversal might be, at least partially, a cyclonic re-circulation of the Benguela Current. Such a re-circulation, yet closer to the coast, was observed by Moroshkin et al. (1970), who reported a branch of the Benguela Current extending northward to 14°S east of 10°E, then re-

circulating southward along the African coast. Lass et al. (2000) observed a 6 x 10^6 m^3 s^{-1} eastward jet impinging on to the African coast at about 14°S that might be connected to the northern limb of this inferred southern cyclonic circulation. A recent estimate of the mean velocity at 7°W derived from float trajectories at about 750 m depth in the Benguela Current extension (Richardson and Garzoli, 2001) reveals an eastward flow between 18°S and 21°S, which also substantiates the existence of an eastward re-circulation of the Benguela Current south of the Angola Gyre.

The zero crossing of the cumulative transport curve for A13 occurs at 26°S, south of the tropical/subtropical transitions at 16°S-24°S previously inferred from the tracers (section 3.2). Although this might be due to the aforementioned presence of a mesoscale dipole, it more likely reflects the effect of the poleward current that results in an alongslope inter-gyre transport of typically 3 x 10^6 m^3 s^{-1} (Garzoli and Gordon, 1996).

6.2 The subtropical gyre

Boxes I and II provide independent estimates of the Benguela and South Atlantic Current transports (Table 5). At 9°W, taking the northern limit of the Benguela Current at the zero crossing of the transport curve at 19°15'S and the southern limit at the location of the Benguela-South Atlantic Current oxygen front at 35°30'S (Figs. 8 and 3), we estimate 32 ± 4 x 10^6 m^3 s^{-1} westward for the upper-layer transport of the Benguela Current. Between 35°30'S and 40°30'S, the South Atlantic Current carries 10 ± 5 x 10^6 m^3 s^{-1} (Fig. 8). To the south of 40°30'S and up to the intersection with A11, the transport is westward. Along A11, eddy-like features in the transport curve are identified between 9°W and 5°E, but the trend gives a transport of 12 x 10^6 m^3 s^{-1} associated with the South Atlantic Current, an estimate similar to that across 9°W. East of 5°E, the 31 ± 12 x 10^6 m^3 s^{-1} northward transport across A11 is assigned to the Benguela Current (Fig. 8).

Now considering Box II, the net upper-layer transport across the Cape Town line is 18 x 10^6 m^3 s^{-1} northward (Fig. 9). The STF is located at 12°E (Fig. 5), and the net flow to the west of 13°E is directed south-eastward (east of the Agulhas ring at 10-11°E). This suggests taking 13°E as the western limit of the Benguela Current along the Cape Town line, which leads to a

transport of $22 \pm 7 \times 10^6$ m^3 s^{-1} northward for the Benguela Current and a southward transport of $3 \pm 6 \times 10^6$ m^3 s^{-1} for the South Atlantic Current. Along A13, taking the latitude 38°S as the limit between the South Atlantic Current and the Benguela Current (Fig.4), we find a transport of $9 \pm 3 \times 10^6$ m^3 s^{-1} eastward for the former and $28 \pm 4 \times 10^6$ m^3 s^{-1} westward for the latter (Fig. 9). As for A14, the northern limit of the Benguela Current is taken at the zero-crossing of the cumulative transport curve at 25°30'S, which excludes from the Benguela Current transport estimate the contribution of water re-circulating eastward in the tropical gyre.

Given the associated error bars, our estimates of the Benguela Current transports across A13 and A14 are similar (Table 5). They compare well with the transport estimates obtained from hydrography by Stramma and Peterson (1989) (26×10^6 m^3 s^{-1} for the Benguela Current at 30°S in the upper 1000 m) and Gordon et al. (1992) (25×10^6 m^3 s^{-1} found at 30°S in the upper 1500 m). They are, however, significantly larger than those proposed by Garzoli and Gordon (1996) and Garzoli et al. (1996) from inverted echo sounders and current meter measurements, which indicated a Benguela Current mean transport of $16 \pm 1 \times 10^6$ m^3 s^{-1} for 1993 – 1996 in the upper 1000 m at 30°S. One possible reason for this disagreement could be that the Garzoli et al. (1996) observations did not resolve the part of the Benguela Current transport lying against the African shelf. Our estimates of the South Atlantic Current transports of $9 – 12 \times 10^6$ m^3 s^{-1} are on the low side compared to those compiled by Smythe-Wright et al. (1998), who find South Atlantic Current transports in the range $11 - 28 \times 10^6$ m^3 s^{-1} for the upper 1500 m in the Cape Basin. Given the uncertainties, they are compatible with the 15×10^6 m^3 s^{-1} reported by Stramma and Peterson (1990) for the South Atlantic Current transport in the eastern Cape Basin.

7. Summary and Discussion

7.1 Equatorial and subequatorial circulations

The new observations provided by A13 and A14 confirm the equatorial circulation patterns proposed by Stramma and England (1999) (Fig. 2). The current structures observed east of the Mid-Atlantic Ridge at 9°W are similar to those of the western basin. At the approach of the eastern boundary the EUC re-circulates into the northern and equatorial branches of the SEC.

During the cruise, some re-circulation into the equatorial SEC was taking place east of 2°E (A13), a slight difference with the pattern of Figure 2, and there are indications that the supply to the Gabon-Congo Current was limited. In the subequatorial domain, the SEUC, which was identified as an undercurrent at 9°W (A14), was surface-intensified at 5°E (A13) by the contribution of the Angola Gyre surface flow. There are indications from the oxygen measurements of an identifiable SECC contribution to the Angola Gyre northern limb at 5°E (A13), another possible adjustment to Figure 2. The set of eastward currents located between the equator and 13°S contributes to the Angola Current, whose transport was estimated at 16 x 10^6 m^3 s^{-1}. The finding of cumulative transport and salinity maxima at 13°S on both A13 and A14, associated with northward oxygen gradients in the upper Central Water (100 m-300 m depth), bears out the idea of a cyclonic subequatorial gyre extending westward beyond the Angola Gyre proper, probably to the vicinity of the ocean western boundary. This is schematized in Figure 2 by the basin-wide triangular circulation formed of the SECC, the Angola Current and the southern SEC branch, yet our analysis suggests that an eastward flow at 16°S-17°S within this basin-wide pattern should also complement the schematics. This eastward current is mostly developed at the intermediate level. Gordon and Bosley's (1991) dynamic height map at 500 db presents such a circulation that was interpreted as a southward shift of the deep part of the Angola Gyre. From the property analyses and transport calculation we rather see this flow as a partial re-circulation of the Benguela Current.

A poleward undercurrent transfers mass between the tropical and sub-tropical South Atlantic (Nelson, 1989; Gordon et al., 1995; Shannon and Nelson, 1996). We noted that the zero-crossing of the integrated transport curve for A13, which marks the southern limit of a net poleward transport inshore of that line, is at 25°30'S (Fig.9). This being clearly south of the surface expression of the Angola-Benguela Front, as of the other subsurface gradients that mark the tropical/subtropical transition along A13, is indicative of a mass transfer between the tropics and subtropics, and indirectly supports the existence of a poleward undercurrent. The inferred transport between the tropics and subtropics ranges between 2 x 10^6 and 5 x 10^6 m^3 s^{-1} in the transition latitudinal range 18°S-22°S (Fig. 9).

7.2 Contributions to the Benguela Current

Determining the origin of the Benguela Current is still a subject of debate related to the South Indian-South Atlantic Oceans water exchanges (Gordon, 1986; Gordon, et al. 1992). Several studies (Stramma and Peterson, 1990; Gordon et al., 1992; Garzoli et al., 1996; Garzoli and Gordon, 1996) identified the South Atlantic and the Agulhas Currents as sources of the Benguela Current but they sometimes disagree about the respective shares of these currents. Gordon et al. (1992), from an analysis based on geostrophic transport estimates and water mass mixing using oxygen and chlorofluorocarbon concentrations, estimated that 60% of the Benguela Current originates from the Agulhas Current and 40% from the South Atlantic Current. Garzoli et al. (1996), considering the 1993-96 average, concluded that 50% of the Benguela Current water comes from the South Atlantic Current, 25% from the Agulhas Current and 25% from the tropics. However, the variability around the mean is large and might explain discrepancies between the Gordon et al. and Garzoli et al. estimates. For instance, Garzoli et al. (1996) noted that, in 1995, the situation was atypical with more that 50% of the Benguela Current transport originating from the Indian Ocean, about 30 % from the South Atlantic Current, and 20% from the tropics. Also, the Garzoli et al. (1996) estimates were based on flow direction rather than water mass analysis.

The amount of South Atlantic water entering Box II is 6 x 10^6 m^3 s^{-1}. This input joins the Benguela Current north of the Cape Town Line (Table 5). This estimate is half the transport of the South Atlantic Current across A11 (Table 5) implying that about half of the South Atlantic Current that crossed A11 southeastward heads towards the Agulhas retroflection where it is expected to, at least in part, mix with Agulhas water (Boebel et al., 2003) and subsequently flow northward into the Benguela Current. Indeed, the Benguela Current off Cape Town carries Indian Ocean water mixed with South Atlantic water (Gordon et al., 1992). Assuming that the 12 x 10^6 m^3 s^{-1} of South Atlantic Current water eventually join the Benguela Current (half north of the Cape Town Line, half south) and noting that we do not resolve the mass transport by the mesoscale circulation, the contributions to the Benguela Current transport (28 x 10^6 m^3 s^{-1}) would be ~ 40% (12x10^6 m^3 s^{-1}) for the South Atlantic, ~ 50% (15 x 10^6 m^3 s^{-1}) for the Indian Ocean, complemented by a 10% input of tropical water at lower latitudes, taking 3 x 10^6 m^3 s^{-1} as an average tropical/subtropical exchange. This crude breakdown of the current roughly matches that of Gordon et al. (1992). Our hypothesis that most of the South Atlantic Current water joins the Benguela Current might seem in

contradiction with Gordon at al. (1992) who argued that part of the South Atlantic Current circulates into the Indian Ocean. Those authors, however, used a definition for the South Atlantic Current that included a contribution from the Drake Passage that was the main source of water proceeding to the Indian Ocean.

7.3 Temporal variability

Although Box I was formed of data subsets acquired two years apart (yet from the same season), the compatibility of the solution for this Box with that of Box II allows us to regard the solution as representative of the period January-March 1995. We should note, however, that variations of the circulation at various time scales occur in the geographical domain we have studied. Equatorial jets, particularly the EUC, have long been known to be influenced by seasonal variations. The tight re-circulations of the EUC in the NSEC and ESEC, however, suggest that ignoring possible transient components in this current affects only the equatorial part of the solution. In the Cape Basin, the intersection of intense mesoscale structures by the hydrographic sections, though hindering the determination of the subtropical gyre axis along A14, should not affect the net mass transport estimates. These eddies, however, modify the transport distributions along the sections. Considering the Cape Town line, the steep shoreward rising of isotherms visible near the continental slope in the Central and Intermediate waters where the core of the Benguela Current transport is located (Fig.5) raises the question of the existence of a permanent equatorward boundary current. Such a pattern, albeit less abrupt, is also present at the eastern end of A11. This, however, is not a permanent feature, as was revealed by two other realizations of the same transect during cruises A12 and SR2 of the WOCE Hydrographic Programme (not shown). It is unclear from the sole hydrographic sections whether the apparent boundary flow should be regarded as a basic situation frequently masked by neighbouring eddies, or whether the steep isopleths are themselves no more than the signature of an eddy border. A map of altimetric sea surface anomaly showing an eddy tangent to the Cape Town line at the time of the cruise (Arhan et al., 1999) supports the second hypothesis.

At the interannual scale, finally, an El Niño-type variability is known to exist along the African western coast (Hisard, 1980; Shannon et al., 1986), and the year 1995 when A13 and A14 were carried out was indeed anomalous in this respect, with a farther-than-usual

southward extension of the surface saline tropical water along the African coast (Gammelsrød et al., 1998). Our transport estimates should thus be considered as representative of the January-March 1995 period and not of the mean circulation.

7.4 Context of the thermohaline circulation

The exchange of upper-layer water between the South Atlantic Ocean and the South Indian Ocean is expected to balance, in part, the export of North Atlantic Deep Water from the South Atlantic Ocean to the Indian and Pacific Oceans, and contribute to the upper limb of the meridional overturning cell in the Atlantic. Recent estimates of the amplitude of the meridional overturning cell in the South Atlantic obtained from the analysis of the WOCE data set are in the range 15 x 10^6 - 22 x 10^6 m^3 s^{-1} (Saunders and King, 1995; Ganachaud, 1999; Wienders et al., 2000; Holfort and Siedler, 2001; Lux et al., 2001). Our estimate of the Benguela Current upper-layer transport is in the range 28 x 10^6 - 31 x 10^6 m^3 s^{-1} and that of the South Atlantic Current is between 10 x 10^6 and 12 x 10^6 m^3 s^{-1} (Table 5). Assuming that the fraction of the Benguela Current transport that continues into the Brazil Current is not transferred to the subantarctic front at the confluence of the Falkland Current and Brazil Current and recirculates entirely in the South Atlantic Current, the difference between the transport of the Benguela Current and that of the South Atlantic Current should be ascribed to the upper limb of the meridional overturning cell. We find a transport in the range 16 x 10^6 - 19 x 10^6 m^3 s^{-1}, a number very similar to previous estimates.

Acknowledgements: The participation of HM and MA in this work was supported by IFREMER (grant 210161) and INSU/CNRS in the framework of the Programme National d'Etude de la Dynamique du Climat (PNEDC). We thank three anonymous reviewers, whose comments helped us improve the manuscript. We acknowledge the help of P. Le Bot for the preparation of the figures. This is a contribution of the World Ocean Circulation Experiment.

Tables

Water Mass	Abbreviation	Upper Limit	Lower Limit
Surface Water	SW	Surface	$\sigma_0 = 26.2$
Central Water	CW	$\sigma_0 = 26.2$	$\sigma_0 = 27.05$
Intermediate Water	IW	$\sigma_0 = 27.05$	$\sigma_1 = 32.1$
Upper Circumpolar	UC	$\sigma_1 = 32.1$	$\sigma_1 = 32.28$
Deep Water	DW	$\sigma_1 = 32.28$	$\sigma_4 = 45.83$
Lower Deep Water	LDW	$\sigma_4 = 45.83$	$\sigma_4 = 45.92$
Bottom Water	BW	$\sigma_4 = 45.92$	Bottom

Table 1 : Layer definitions (see also Figs. 3, 4, and 5)

Current Name	9°W (A14)	Eastern boundary (A13)
GC		2.7
NSEC	-5.0	-9.9 (-6.9)
EUC	24.6	12.6
ESEC	-5.5	-11.1 (-7.8)
SEUC	7.5	4.7
SECC	4.2	3.3

Table 2 : Zonal transports of equatorial currents from the ADCP. Northern South Equatorial Current (NSEC), Equatorial Undercurrent (EUC), South Equatorial Undercurrent (SEUC), Guinea Current (GC), South Equatorial Countercurrent (SECC), Equatorial South Equatorial Current (ESEC), South Intermediate Countercurrent (SICC). Maximum depth for transport computation for GC and EUC is 190 m or the lower limit of the current, whichever is shallower. It is 300 m or the lower limit of the current, whichever is shallower, for the NSEC, ESEC, SEUC and SECC. The NSEC and ESEC transports between 0 and 190 m are given in parentheses for A13. Transports are in 10^6 m^3 s^{-1} and positive eastward.

Constraint	Imposed Value	Comment
surface-to-bottom mass conservation	$0 \pm 2.3 \times 10^9$ kg s^{-1}	
surface-to-bottom heat conservation	$(0.4 \pm 0.4) \times 10^{15}$W	
surface-to-bottom salt conservation	$0 \pm 80 \times 10^9$ kg s^{-1}	
surface-to-bottom silicate conservation	$0 \pm 92 \times 10^9$ µmol s^{-1}	
heat, salt and silicate conservations in layers 2 to 8	$0 \pm K_{v0} \cdot A \cdot \frac{\partial \Phi}{\partial z}$	
EUC transport	$(20.5 \pm 2.5) \times 10^6$ m^3 s^{-1}	$\sigma_0 < 26.2$ between 2°S and 2°N
SEUC transport	$(7.3 \pm 2.2) \times 10^6$ m^3 s^{-1}	$27.05 < \sigma_0 < 26.2$ between 3° and 5°S
SECC transport	$(4.2 \pm 0.7) \times 10^6$ m^3 s^{-1}	$27.05 < \sigma_0 < 26.2$ between 8°S and 9°30'S
LDW transport between the African coast and 4°30'S from Lux et al. (2001)	$(4.0 \pm 2.0) \times 10^6$ m^3 s^{-1}	$45.83 < \sigma_4 < 45.92$

Table 3: Constraint setting for Box I (A14-A11). Transports are positive eastward. K_{v0} is the a priori value of the vertical diffusivity. A is the area of the given layer interface and $\frac{\partial \Phi}{\partial z}$ the vertical gradient of the given tracer.

Constraint	Imposed Value	Comment
surface-to-bottom mass conservation	$(0 \pm 2.5) \times 10^{9}$ kg s^{-1}	
surface-to-bottom heat conservation	$(0.1 \pm 0.3) \times 10^{15}$W	
surface-to-bottom salt conservation	$0 \pm 87 \times 10^{9}$ kg s^{-1}	
surface-to-bottom silicate conservation	$0 \pm 100 \times 10^{9}$ µmol s^{-1}	
heat, salt and silicate conservations in layers 2 to 8	$0 \pm K_{v0} \cdot A \cdot \frac{\partial \Phi}{\partial z}$	
GC	$(2.2 \pm 0.9) \times 10^{6}$ m^3 s^{-1}	$\sigma_0 < 26.2$ north of 4°N
NSEC transport	$(-4.6 \pm 2.5) \times 10^{6}$ m^3 s^{-1}	$\sigma_0 < 26.2$ between 1° and 3°23'N
EUC transport	$(6.3 \pm 2.4) \times 10^{6}$ m^3 s^{-1}	$\sigma_0 < 26.2$ between 1°20'S and 1°N
ESEC transport	$(-7.1 \pm 2.8) \times 10^{6}$ m^3 s^{-1}	$\sigma_0 < 26.2$ between 4° and 1°20'S
transport between 4°-6°S	$(5.8 \pm 3.5) \times 10^{6}$ m^3 s^{-1}	$\sigma_0 < 27.05$ between 4° and 6°S

Table 4 : Constraint setting for Box II (A13-Cape Town line). Transports are positive eastward. K_{v0} is the a priori value of the vertical diffusivity. A is the area of the given layer interface and $\frac{\partial \Phi}{\partial z}$ the vertical gradient of the given tracer.

Benguela Current Transport			
9°W from A14	30°S from A11	10°E from A13	35°S from the Cape Town line
-32 ± 4	-31 ± 12	-28 ± 4	22 ± 7
South Atlantic Current Transport			
9°W from A14	30°S from A11	A13	Cape Town line
10 ± 5	-12 ± 10	9 ± 3	-3 ± 6

Table 5. Benguela Current and South Atlantic Current transports from inverse models S1 for $\sigma_1 < 32.1$. Transports and error estimates are in 10^6 m^3 s^{-1}. Positive values indicate eastward or northward transports.

References

Arhan, M., Mercier, H., Bourlès, B., Gouriou, Y., 1998. Hydrographic sections across the Atlantic at 7°30N and 4°30S. Deep-Sea Research I 45, 829-872.

Arhan, M., Mercier, H., Lutjeharms, J.R.E., 1999. The disparate evolution of three Agulhas rings in the South Atlantic Ocean. Journal of Geophysical Research 104, 20987-21005.

Boebel, O., Davis, R.E., Ollitrault, M., Peterson, R.G., Richardson, P.L., Schmid, C., Zenk, W., 1999. The intermediate depth circulation of the western south Atlantic. Geophysical Research Letters 26, 3329-3332.

Boebel, O., Lutjeharms, J., Schmid, C., Zenk, W., Rossby, T., Barron, C., 2003. The Cape Cauldron: a regime of turbulent inter-ocean exchange. Deep-Sea Research II 50, 57-86.

Bourlès, B., Gouriou, Y., Chuchla, R., 1999. On the circulation in the upper layer of the western equatorial Atlantic. Journal of Geophysical Research 104, 21151-21170.

Bubnov, V.A., 1972. Structure and characteristics of the oxygen minimum layer in the southeastern Atlantic. Oceanology 12, 193-201.

Bubnov, V.A., Egorikhin, V.D., 1980. Study of water circulation in the tropical Atlantic. Deep-Sea Research Part A 26 (Suppl. II), 125-136.

Chapman, P., Shannon, L.V., 1987. Seasonality in the oxygen minimum layers at the extremities of the Benguela system. South African Journal of Marine Sciences 5, 85-94.

Gammelsrød, T., Bartholomae, C.H., Boyer, D.C., Filipe, V.L.L., O'Toole, M.J., 1998. Intrusion of warm surface layers along the Angolan-Namibian coast in February-March 1995 : The 1995 Benguela Niño. South African Journal of Marine Science 19, 41-56.

Ganachaud, A., 1999. Large scale oceanic circulation and fluxes of freshwater, heat, nutrients and oxygen. Doctoral dissertation, Massachusetts Institute of Technology – Woods Hole Oceanographic Institution, 266 pp.

Ganachaud, A., submitted. Error budget of inverse models: The North Atlantic. Submitted to Journal of Atmospheric and Oceanographic Technology.

Garzoli, S.L., Gordon, A.L., 1996. Origins and variability of the Benguela Current. Journal of Geophysical Research 101, 897-906.

Garzoli, S.L., Gordon, A.L., Kamenkovich, V., Pillsbury, D., Duncombe-Rae, C., 1996. Variability and sources of the southeastern Atlantic circulation. Journal of Marine Research 54, 1039-1071.

Gordon, A.L., 1986. Interocean exchanges of thermocline water. Journal of Geophysical Research 91, 5037-5046.

Gordon, A.L., Bosley, K.T., 1991. Cyclonic gyre in the tropical South Atlantic. Deep-Sea Research 38 (Suppl.), S323-S343.

Gordon, A.L., Weiss, R.F., Smethie, Jr. W.M., Warner, M., 1992. Thermocline and intermediate water communication between the South Atlantic and Indian oceans. Journal of Geophysical Research 97, 7223-7240.

Gordon, A.L., Bosley, K.T., Aikman, F., 1995. Tropical Atlantic water within the Benguela upwelling system at 27°S. Deep-Sea Research I 42, 1-12.

Groupe Cither 3 (Le), 1996a. Campagne CITHER 3, Recueil de données, Vol. 2: $CTDO_2$, Rapport Interne LPO 96-05, 533 pp., Laboratoire de Physique des Océans, IFREMER centre de Brest, France.

Groupe Cither 3 (Le), 1996b. Campagne CITHER 3, Recueil de données, Vol. 3: Traceurs Géochimiques, Rapport Interne LPO 98-03, 587 pp., Laboratoire de Physique des Océans, IFREMER centre de Brest, France.

Hisard, P., 1975. La circulation superficielle dans la partie occidentale du Golfe de Guinée. Documents Scientifiques Du Centre de Recherche Océanographique d'Abidjan 6, 41-57.

Hisard, P., 1980. Observations de réponses de type « El Niño » dans l'Atlantique tropical oriental Golfe de Guinée. Oceanologica Acta 3, 69-78.

Holfort, J., Siedler, G., 2001. The meridional oceanic transports of heat and nutrients in the South Atlantic. Journal of Physical Oceanography 31, 5-29.

Lass, H.U., Schmidt, M., Mohrholz, V., Nausch, G., 2000. Hydrographic and current measurements in the area of the Angola-Benguela front. Journal of Physical Oceanography 30, 2589-2609.

Lux, M., Mercier, H., Arhan, M., 2001. Interhemispheric exchanges of mass and heat in the Atlantic Ocean in January-March 1993. Deep-Sea Research I 48, 605-638.

Meeuwis, J.M., Lutjeharms, J.R.E., 1990. Surface thermal characteristics of the Angola-Benguela front. South African Journal of Marine Science 9, 261-279.

Mémery, L., Arhan, M., Alvarez-Salgado, X.A., Messias, M.J., Mercier, H., Castro, C.G., Rios, A.F., 2000. The water masses along the western boundary of the South and Equatorial Atlantic. Progress in Oceanography 47, 69-98.

Mercier, H., 1986. Determining the general circulation of the ocean: a nonlinear inverse problem. Journal of Geophysical Research 91, 5103-5109.

Molinari, R.L., 1982. Observations of eastward currents in the tropical South Atlantic ocean : 1978-1980. Journal of Geophysical Research 87, 9707-9714.

Mohrholz, V., Schmidt, M., Lutjeharms, J.R.E., 2001. The hydrographic and dynamics of the Angola-Benguela frontal zone and environment in April 1999. South African Journal of Marine Science 95, 199-208.

Moroshkin, K.V., Bubnov, V.A., Bulatov, R.P., 1970. Water circulation in the eastern South Atlantic. Oceanology 10, 27-34.

Nelson, G., 1989: Poleward motion in the Benguela area. In Neshbya, S.J., Mooers, Ch.N.K., Smith, R.L., Barber, R.T. (Eds.), Poleward flows along eastern ocean boundaries. Springer-Verlag, pp110-130.

Polzin, K.L., Toole, J.M., Ledwell, J.R., Schmitt, R.W., 1997. Spatial variability of turbulent mixing in the Abyssal Ocean. Science 276, 93-96.

Richardson, P.L., Garzoli, S.L., 2001. Characteristics of Intermediate water flow in the Benguela Current as measured with RAFOS floats. Submitted.

Saunders, P.M., King, B.A., 1995. Oceanic fluxes on the WOCE A11 Section. Journal of Physical Oceanography 25, 1942-1958.

Shannon, L.V., Boyd, A.J., Brundrit, G.B., Taunton-Clark, J., 1986. On the existence of an EL Niño-type phenomenon in the Benguela system. Journal of Marine Research 44, 495-520.

Shannon, L.V., Nelson, G., 1996. The Benguela: Large scale features and processes and system variability. In : Wefer, G., Berger, W.H., Siedler, G., Webb, D. J. (Eds.), The South Atlantic: present and past circulation. Springer, 644 pp.

Smythe-Wright, D., Chapman, P., Duncombe Rae, C., Shannon, L.V., Biswell, S.W., 1998. Characteristics of the South Atlantic subtropical frontal zone between 15°W and 5°E. Deep-Sea Research I 45, 167-192.

Speer, K.S., Siedler, G., Talley, L., 1995. The Namib Col Current. Deep-Sea Research I 42, 1933-1950.

Stramma, L., England, M., 1999. On the water masses and mean circulation of the South Atlantic Ocean. Journal of Geophysical Research Oceans 104, 20863-20883.

Stramma, L., Peterson, R.G., 1989. Geostrophic transport in the Benguela Current Region. Journal of Physical Oceanography 19, 1440-1448.

Stramma, L., Peterson, R.G., 1990. The South Atlantic Current. Journal of Physical Oceanography, 20, 846-859.

Stramma, L., Schott, F., 1996. Western equatorial circulation and interhemispheric exchange. In: Krauss, W. (Ed.), The warmwatersphere of the North Atlantic Ocean. Gebrüder Borntraeger, Berlin, 446pp.

Stramma, L., Schott, F., 1999. The mean flow field of the tropical Atlantic Ocean. Deep-Sea Res. II 46, 279-303.

Suga, T., Talley, L.D., 1995. Antarctic Intermediate Water circulation in the tropical and subtropical South Atlantic. Journal of Geophysical Research 100, 13441-13353.

Tarantola, A., Valette, B., 1982. Generalized nonlinear problems solved using the least squares criterion. Review of Geophysics, 20, 219-232.

Tomczak, M., Godfrey, J.S., 1994. Regional Oceanography: An introduction. Pergamon, 422 pp.

Tsuchiya, M., 1986. Thermostads and circulation in the upper layer of the Atlantic Ocean. Progress in Oceanography 16, 235-267.

Tsuchiya, M., Talley, L.D., McCartney, M.S., 1994: Water mass distributions in the western South Atlantic; A section from South Georgia (54S) northward across the equator. Journal of Marine Research, 52, 55-81.

Voituriez, B., 1981. Les sous-courants équatoriaux nord et sud et la formation des dômes thermiques tropicaux. Oceanologica Acta, 4, 497-506.

Wacongne, S., Piton, B.,1992. The near-surface circulation in the northeastern corner of the South Atlantic Ocean. Deep-Sea Research 39, 1273-1298.

Warren, B.A., Speer, K.G., 1991. Deep circulation in the eastern South Atlantic Ocean. Deep-Sea Research 38, Supp., S281-S322.

Whitworth, T. III, Nowlin, W.D., 1987. Water masses and currents of the Southern Ocean at the Greenwich meridian. Journal of Geophysical Research 92, C6, 6462-6476.

Wienders, N., Arhan, M., Mercier, H., 2000. Circulation at the western boundary of the South and Equatorial Atlantic: Exchanges with the ocean interior. Journal of Marine Research 58, 1007-1039.

WOCE Hydrographic Programme Office, 1994. WOCE operation manual. Vol. 3, Part 2.1.3: WHP operations and methods. WHP Office Report, WHPO 91, 1, Revision 1.

Wunsch, C., 1996. The ocean circulation inverse problem. Cambridge University Press, New-York, 437pp.

Figure Captions

Figure 1: The A11, A13, A14, Ajax and Cape Town hydrographic lines. Dots denote the hydrographic station locations. The names of the main bathymetric features are indicated. Grey shading indicates ocean depths shallower than 3000 m. The closed box made of A14, A11 and the African continent is referred to as Box I. The closed box made of A13, the Cape Town line and the African continent is referred to as Box II.

Figure 2: Schematic of the Equatorial and South Atlantic Ocean circulations at 100-500 m depth adapted from Stramma and England (1999). The A11, A13, A14 and Cape town hydrographic lines are indicated. EUC: Equatorial Undercurrent. NEUC, SEUC : Northern, Southern Equatorial Undercurrent. NSEC, ESEC, CSEC, SSEC : Northern, Equatorial, Central, Southern branches of the South Equatorial Current. NBC, NBUC: North Brazil Current, North Brazil Undercurrent. SECC : South Equatorial Counter Current. AC : Agulhas Current. FC: Falkland Current.

Figure 3: Vertical sections of A) potential temperature (°C), B) salinity and C) dissolved oxygen (μmol kg^{-1}) between 0 and 1400 m along A14. The longitude of A14 varies between 7°W and 9°W. The upper-three layer interfaces defined in Table 1 (σ_0 = 26.2, σ_0 = 27.05, σ_1 = 32.1) are indicated in the potential temperature plot. The σ_0 = 26.3 and σ_1 = 31.85 isopycnals used to describe the meridional property distributions (Fig.6) are shown in the salinity and oxygen plots. SAF : Subantarctic Front. STF : Subtropical Front. SECC : South Equatorial Counter Current. SEUC : South Equatorial Undercurrent. EUC : Equatorial Undercurrent. Upper numbers are station numbers.

Figure 4: Vertical sections of potential temperature (°C), salinity and dissolved oxygen (μmol kg^{-1}) between 0 and 1400 m along A13. The longitude of A13 varies between 1°W and 10°E.The upper three layer interfaces defined in Table 1 (σ_0 = 26.2, σ_0 = 27.05, σ_1 = 32.1) are indicated in the potential temperature plot. The σ_0 = 26.3 and σ_1 = 31.85 isopycnals used to describe the mertidional property distributions (Fig.6) are shown in the salinity and oxygen plots. STF : Subtropical Front. SECC : South Equatorial Counter Current. EUC : Equatorial Undercurrent.

Figure 5: Vertical sections of potential temperature (°C), salinity and dissolved oxygen (μmol kg^{-1}) between 0 and 1400 m along the Cape Town line. The latitude of the section varies between 34°S and 40°S. The upper three layer interfaces defined in Table 1 (σ_0 = 26.2, σ_0 = 27.05, σ_1 = 32.1) are indicated in the potential temperature plot. The σ_0 = 26.3 and σ_1 = 31.85 isopycnals used to describe the meridional property distributions (Fig.6) are shown in the salinity and oxygen plots. STF : Subtropical Front.

Figure 6: Salinity (a) and dissolved oxygen (μmol kg^{-1}) (b) on the σ_0 = 26.3 and σ_1 = 31.85 isopycnal surfaces along the meridional lines A14 (continuous) and A13 (dotted). The σ_0 = 26.3 and σ_1 = 31.85 isopycnals lie in the upper part of the thermocline water layer and in the middle of the intermediate water layer, respectively. The Ajax data are reported in the salinity plots. ABF: Angola-Benguela Front. STF : Subtropical Front. SAF : Subantarctic Front.

Figure 7: The zonal velocity component along A14 (a) and A13 (b) between 4°N and 15°S and between 0 and 800m from the vessel-mounted Acoustic Doppler Current Profiler (ADCP), in 10^{-2} m s^{-1}. Positive values denote eastward movement. EUC: Equatorial Undercurrent. SEUC: Southern Equatorial Undercurrent. NSEC, ESEC : Northern, Equatorial branches of the South Equatorial Current. SECC : South Equatorial Counter Current. GC: Guinea Current. SICC: South Intermediate Counter Current.

Figure 8: Upper-layer (σ_1 < 32.1) cumulative transports along A14 (left) and A11 (right) as estimated from inverse model solution S1 (heavy dark line). The one standard error interval is indicated (grey shading) as well as the a priori solution (dotted line) and estimates obtained as a result of changes in the inverse model settings (see text). Transports (x10^6 m^3 s^{-1}) are positive eastward and northward. The upper-layer transport is defined as the sum of the geostrophic and Ekman transports. The limits of the Benguela Current (BC) and South Atlantic Current (SAC) used for the computations of the transports are indicated. EUC: Equatorial Undercurent. SEUC: South Equatorial Undercurrent. SECC: South Equatorial Countercurrent.

Figure 9: Upper-layer (σ_1 < 32.1) cumulative transports along A13 (left) and the Cape Town line (right) as estimated from inverse model solution S1 (heavy dark line). The one standard error interval is indicated (grey shading) as well as the a priori solution (dotted line). Transports (x10^6 m^3 s^{-1}) are positive eastward and northward. The upper-layer transport is defined as the sum of the geostrophic and Ekman transports. The limits of the Benguela Current (BC) used for the computation of the transport are indicated. EUC: Equatorial Undercurent. SEUC: South Equatorial Undercurrent. AGC: Angola Gyre Center.

Figure 10: Contributions of the surface and thermocline water layers (continuous) and intermediate water layer (dotted) to the cumulative upper-layer transport along A14 and A11 (upper panel) and A13 and the Cape Town line (lower panel). Transports (x10^6 m^3 s^{-1}) are positive eastward and northward. See Table 1 for layer definitions. The surface layer transport is the sum of the geostrophic and Ekman transports. The reader can refer to Figs. 8 and 9 for locations of the main features described in the text.

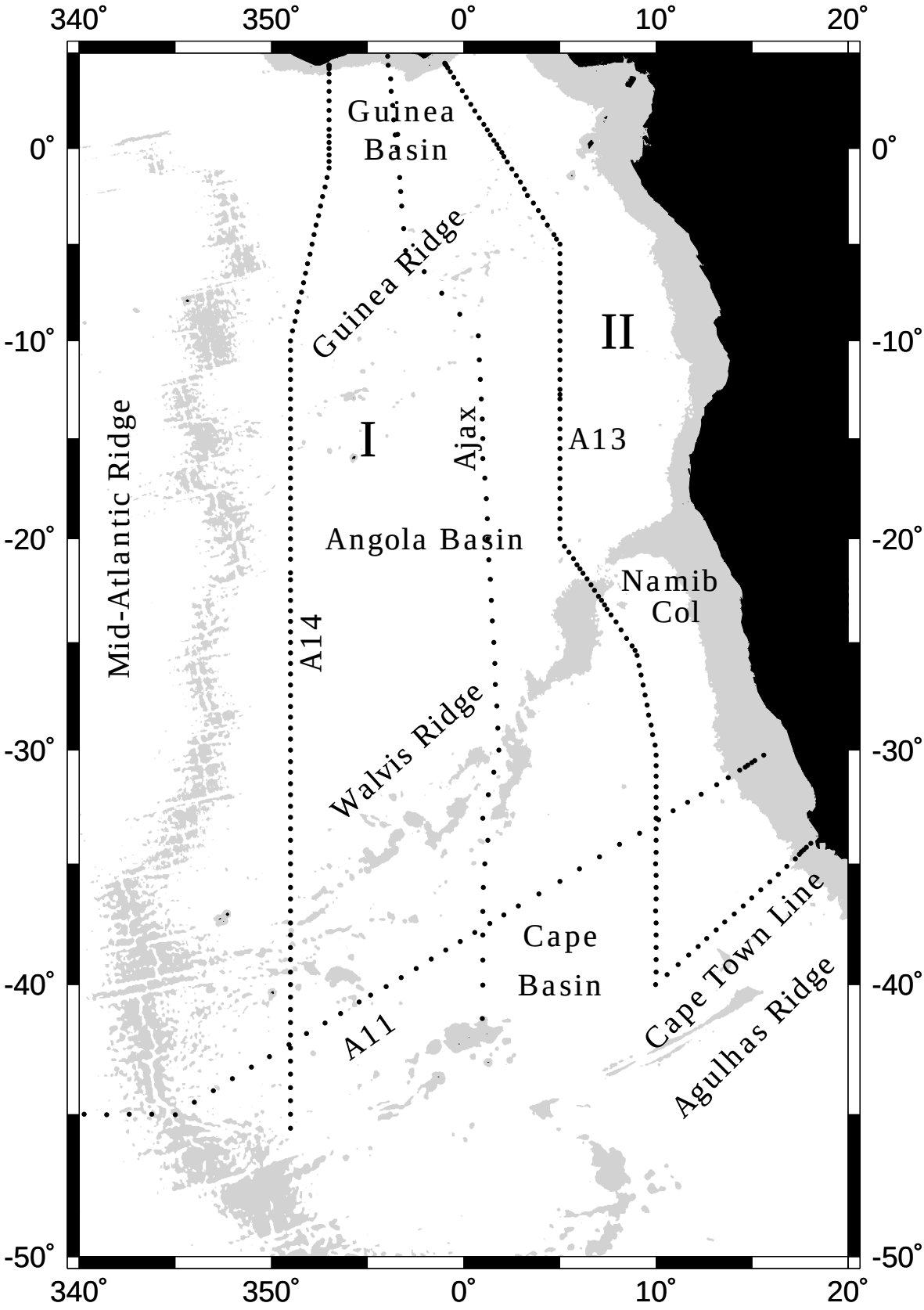
340°
350°
0°
10°
20°
0°
-10°
-20°
-30°
-40°
-50°
Guinea Basin
Guinea Ridge
II
I
Ajax
A13
Mid-Atlantic Ridge
Angola Basin
Namib Col
A14
Walvis Ridge
Cape Basin
A11
Cape Town Line
Agulhas Ridge

FIG 1

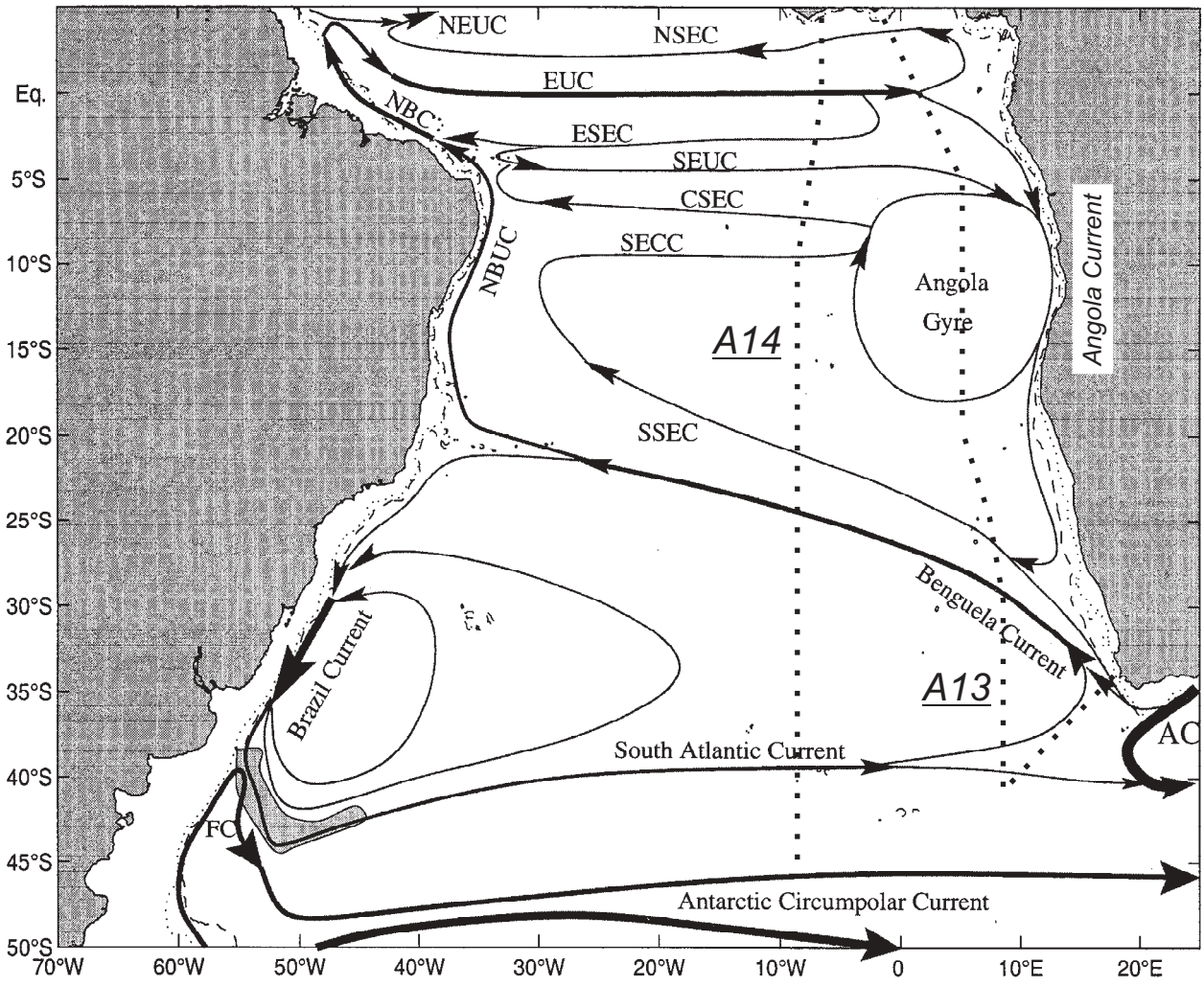
NEUC
NSEC
EUC
NBC
ESEC
SEUC
CSEC
SECC
NBUC
Angola
Gyre
A14
Angola Current
SSEC
Benguela Current
A13
Brazil Current
South Atlantic Current
AC
FC
Antarctic Circumpolar Current
Eq.
5°S
10°S
15°S
20°S
25°S
30°S
35°S
40°S
45°S
50°S
70°W
60°W
50°W
40°W
30°W
20°W
10°W
0
10°E
20°E

FIG 2

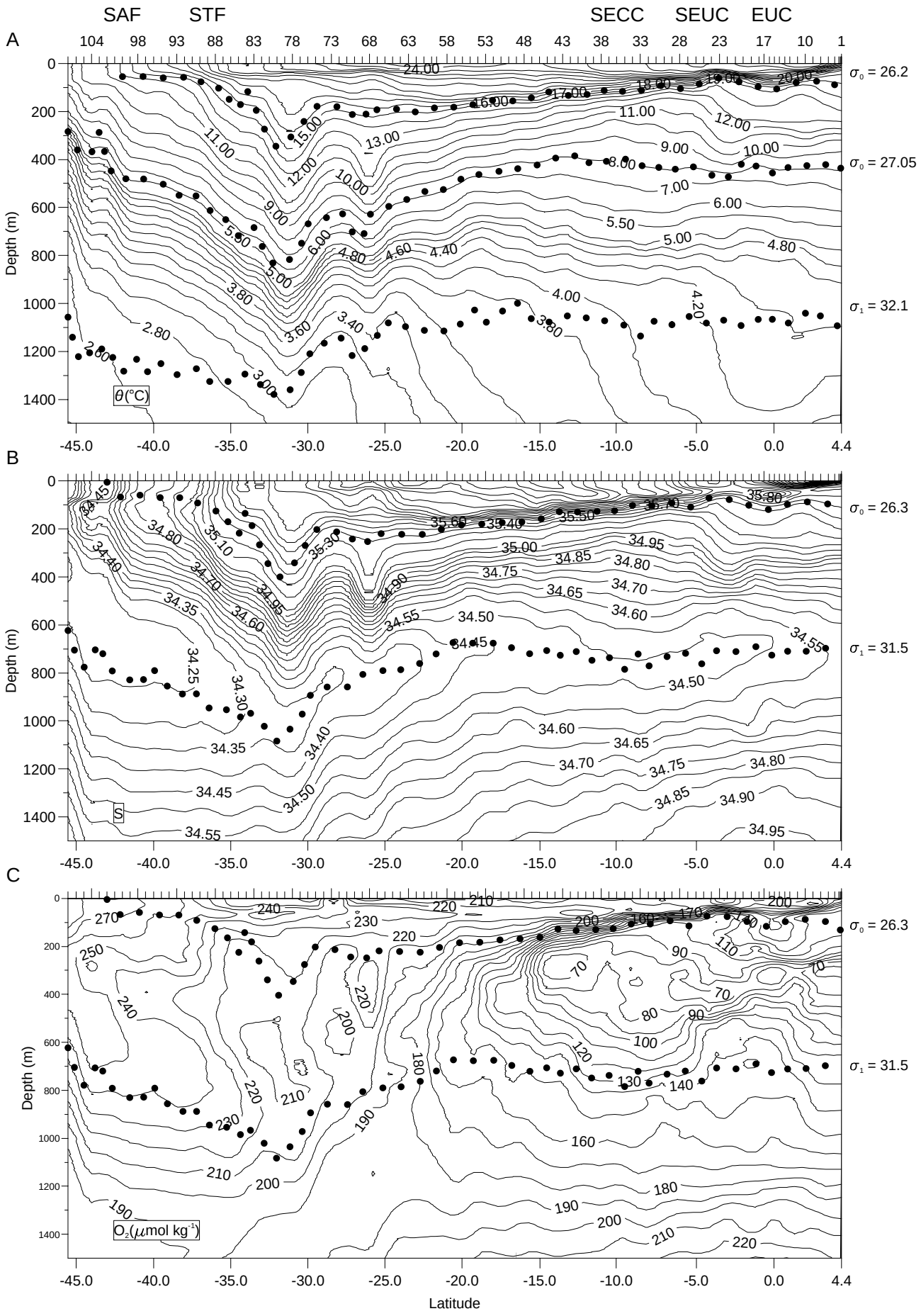
SAF
STF
SECC
SEUC
EUC
A
B
C
104 98 93 88 83 78 73 68 63 58 53 48 43 38 33 28 23 17 10 1
Depth (m)
θ(°C)
S
O2(μmol kg-1)
σ0 = 26.2
σ0 = 27.05
σ1 = 32.1
σ0 = 26.3
σ1 = 31.5
σ0 = 26.3
σ1 = 31.5
-45.0 -40.0 -35.0 -30.0 -25.0 -20.0 -15.0 -10.0 -5.0 0.0 4.4
Latitude

FIG 3

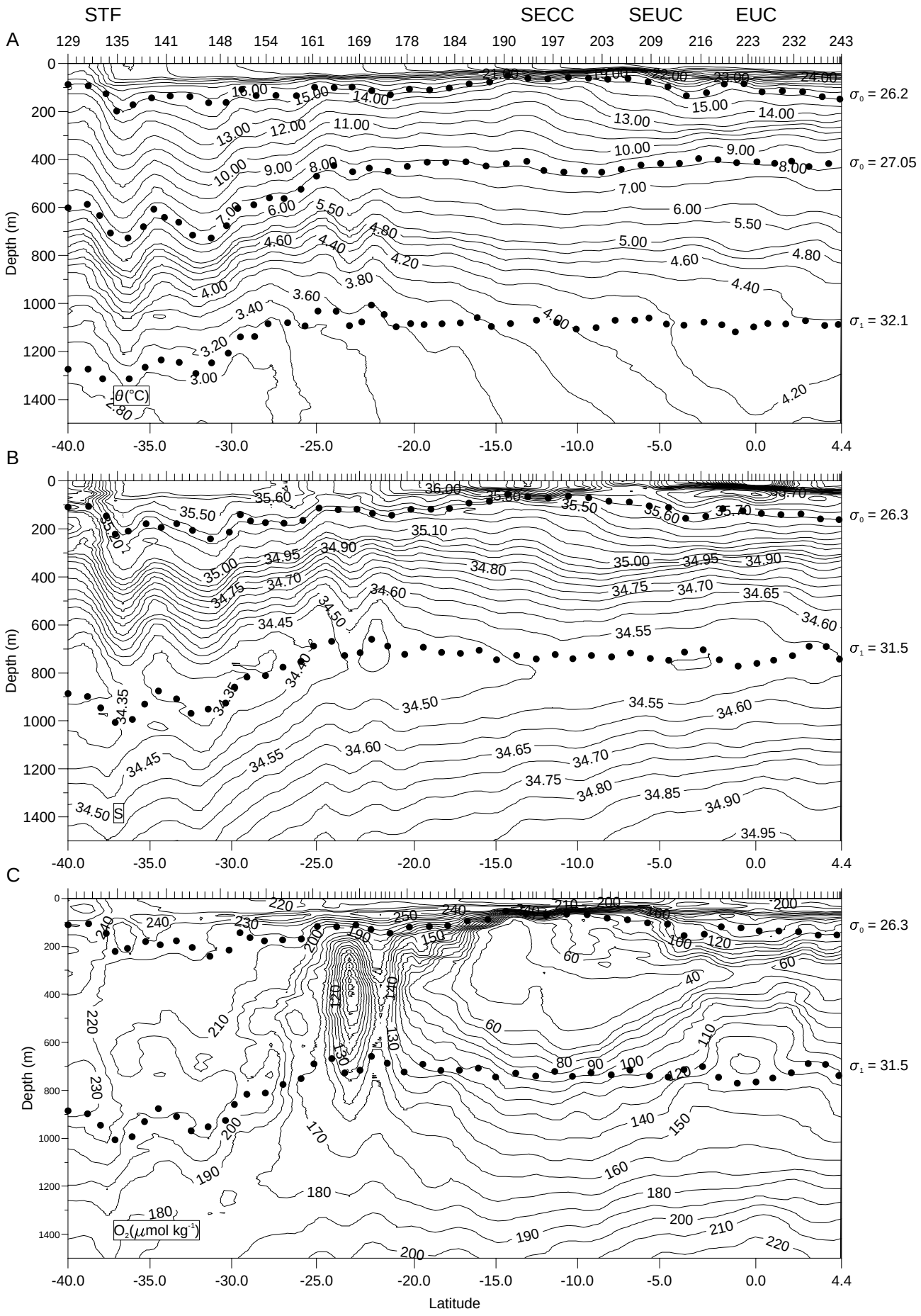
STF
SECC
SEUC
EUC
A
B
C
Depth (m)
Latitude
θ(°C)
S
O₂(μmol kg⁻¹)
σ₀ = 26.2
σ₀ = 27.05
σ₁ = 32.1
σ₀ = 26.3
σ₁ = 31.5
σ₀ = 26.3
σ₁ = 31.5

FIG 4

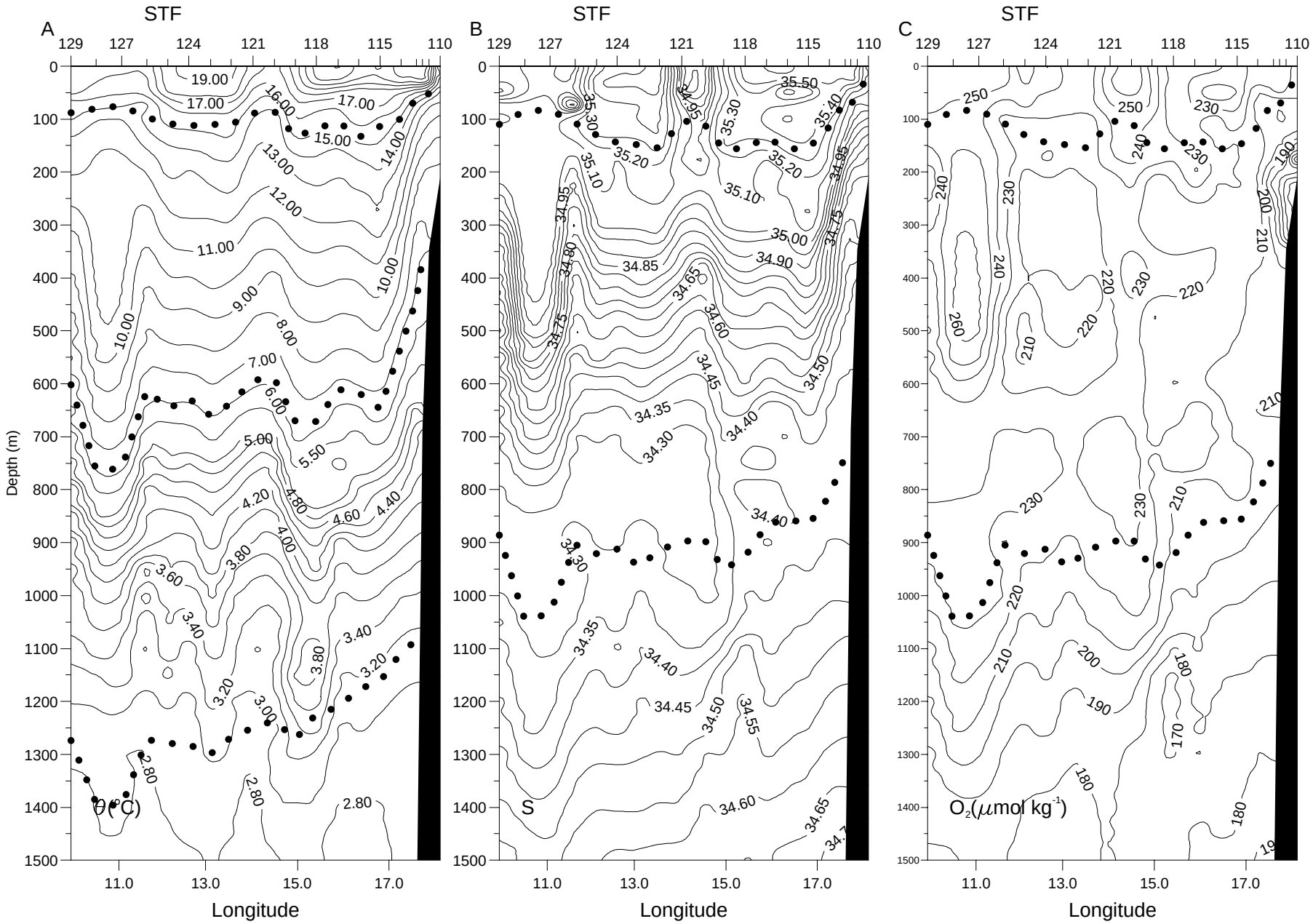
A
STF
B
STF
C
STF
Depth (m)
Longitude
Longitude
Longitude
θ(°C)
S
O2(μmol kg-1)

FIG 5

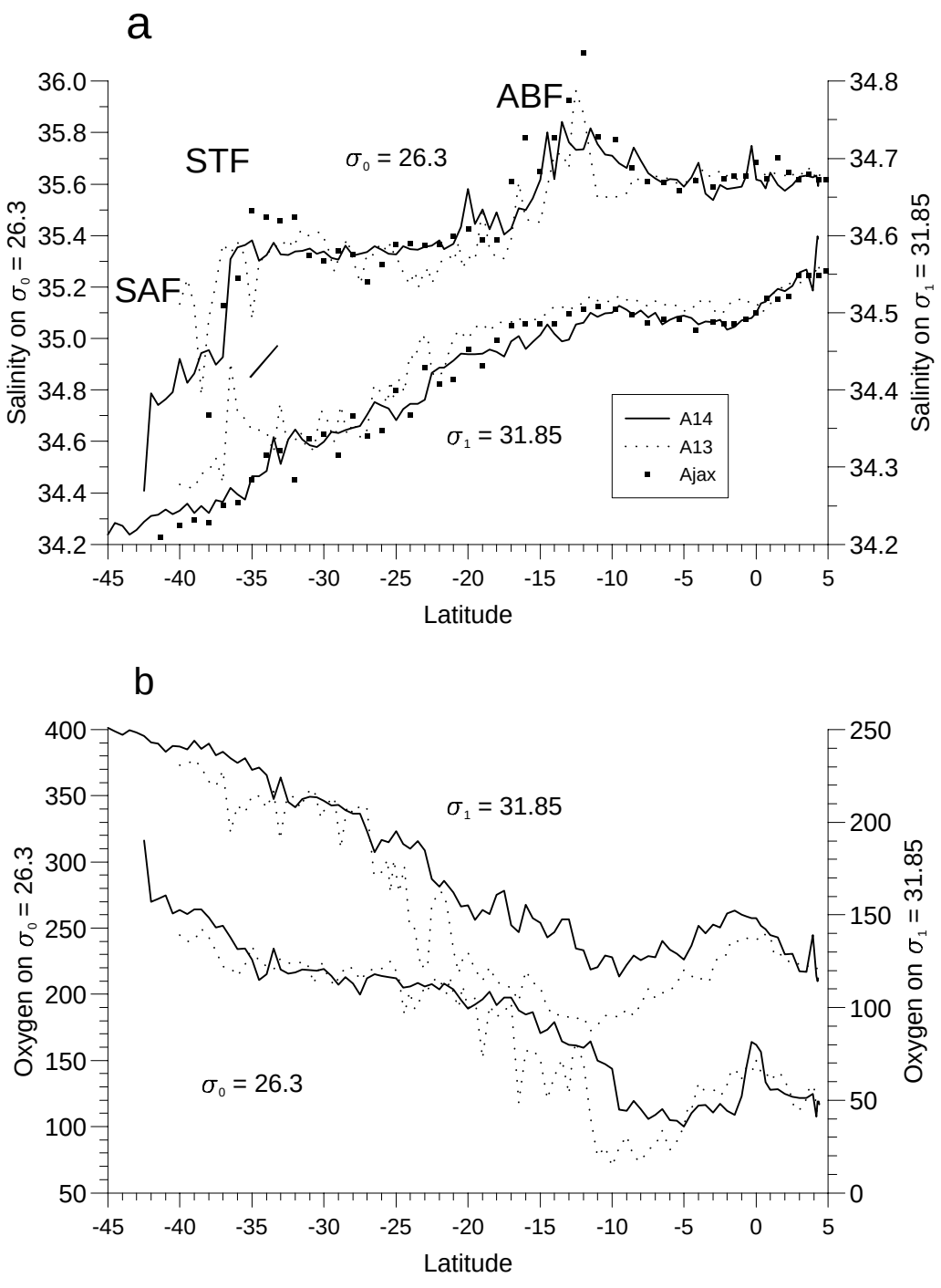
a
ABF
STF
SAF
σ_0 = 26.3
σ_1 = 31.85
A14
A13
Ajax
Salinity on σ_0 = 26.3
Salinity on σ_1 = 31.85
Latitude
b
σ_1 = 31.85
σ_0 = 26.3
Oxygen on σ_0 = 26.3
Oxygen on σ_1 = 31.85
Latitude

FIG 6

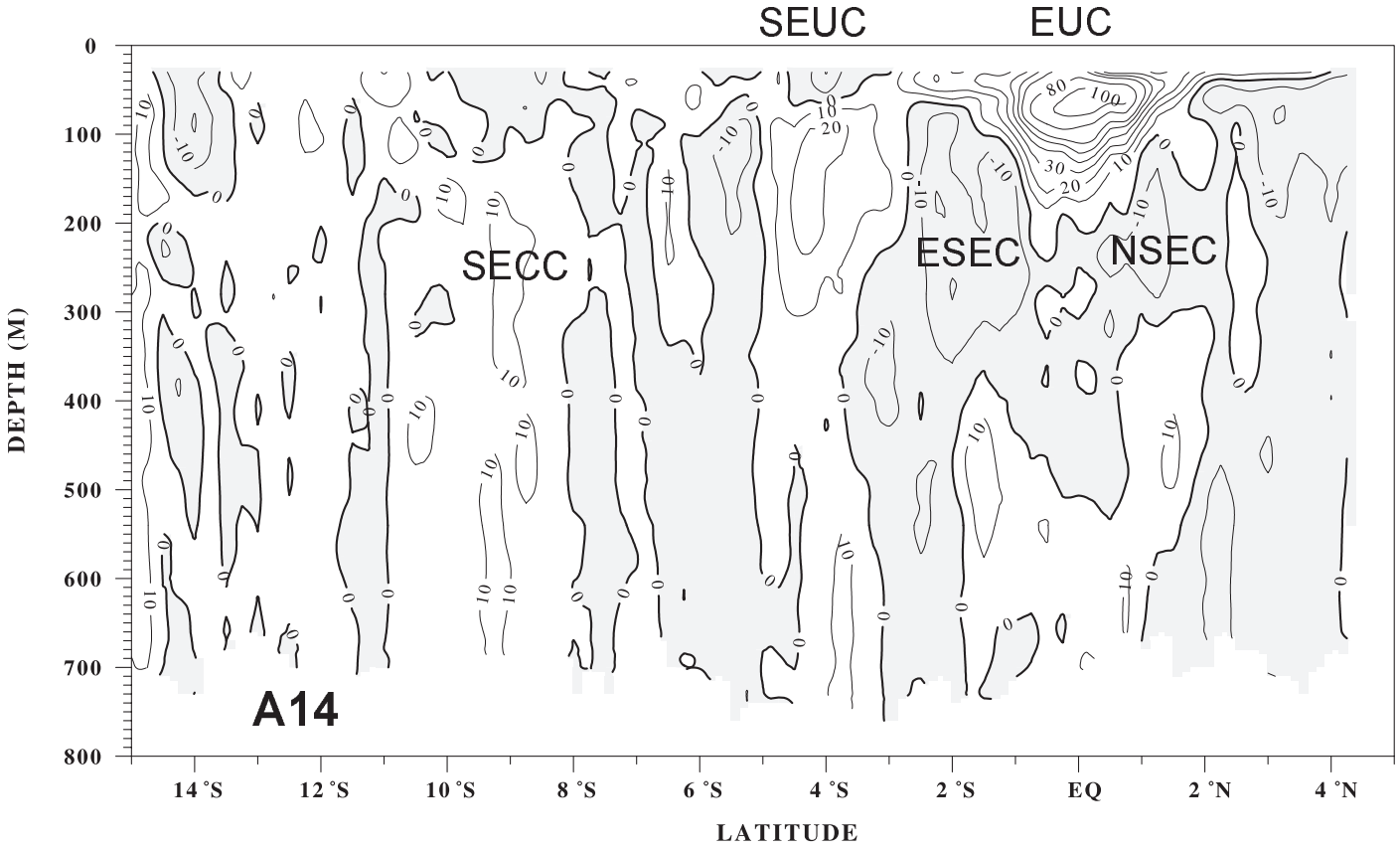
SEUC
EUC
SECC
ESEC
NSEC
A14
DEPTH (M)
0
100
200
300
400
500
600
700
800
14 °S
12 °S
10 °S
8 °S
6 °S
4 °S
2 °S
EQ
2 °N
4 °N
LATITUDE

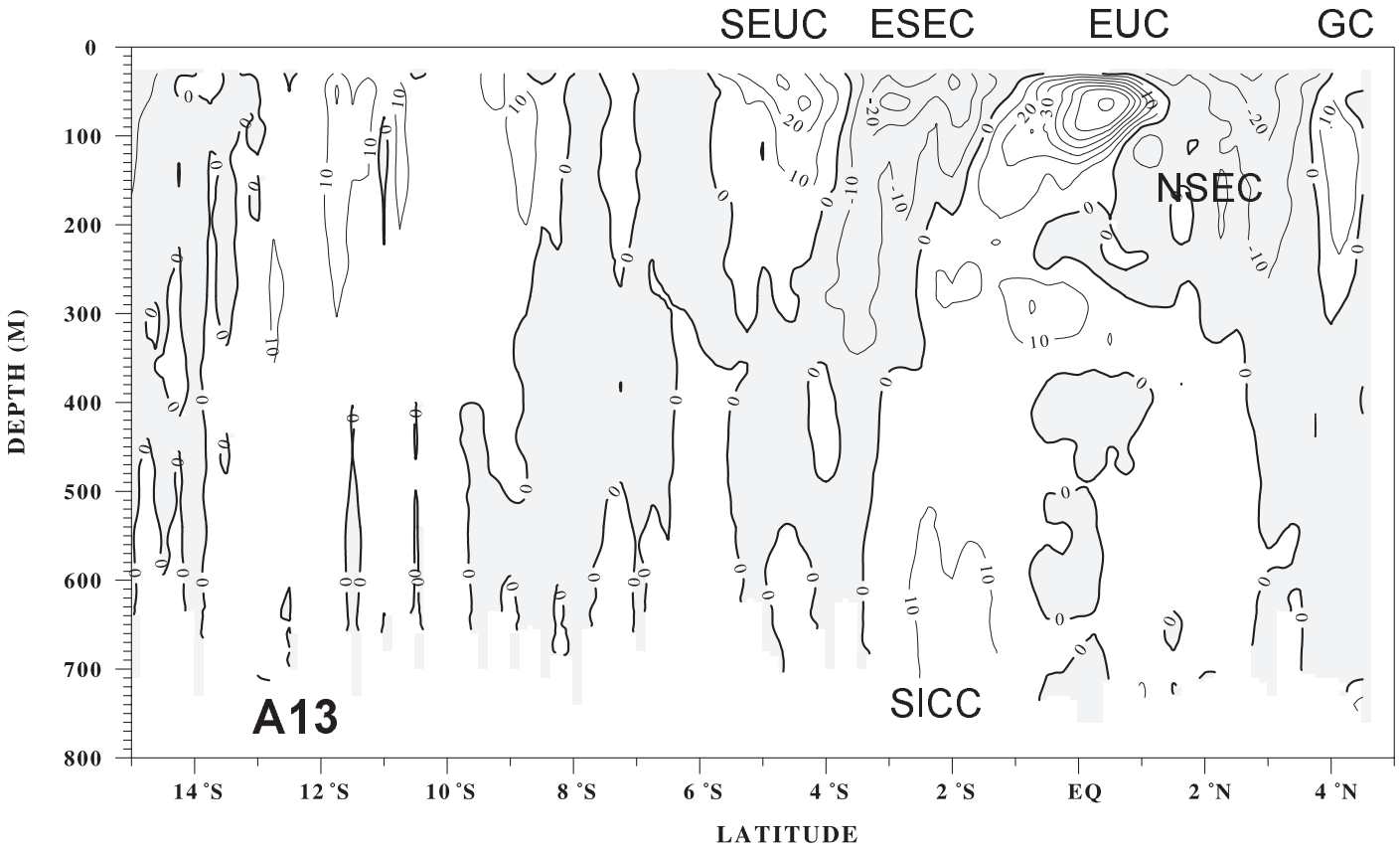
SEUC
ESEC
EUC
GC
NSEC
SICC
A13
DEPTH (M)
0
100
200
300
400
500
600
700
800
14 °S
12 °S
10 °S
8 °S
6 °S
4 °S
2 °S
EQ
2 °N
4 °N
LATITUDE

FIG 7

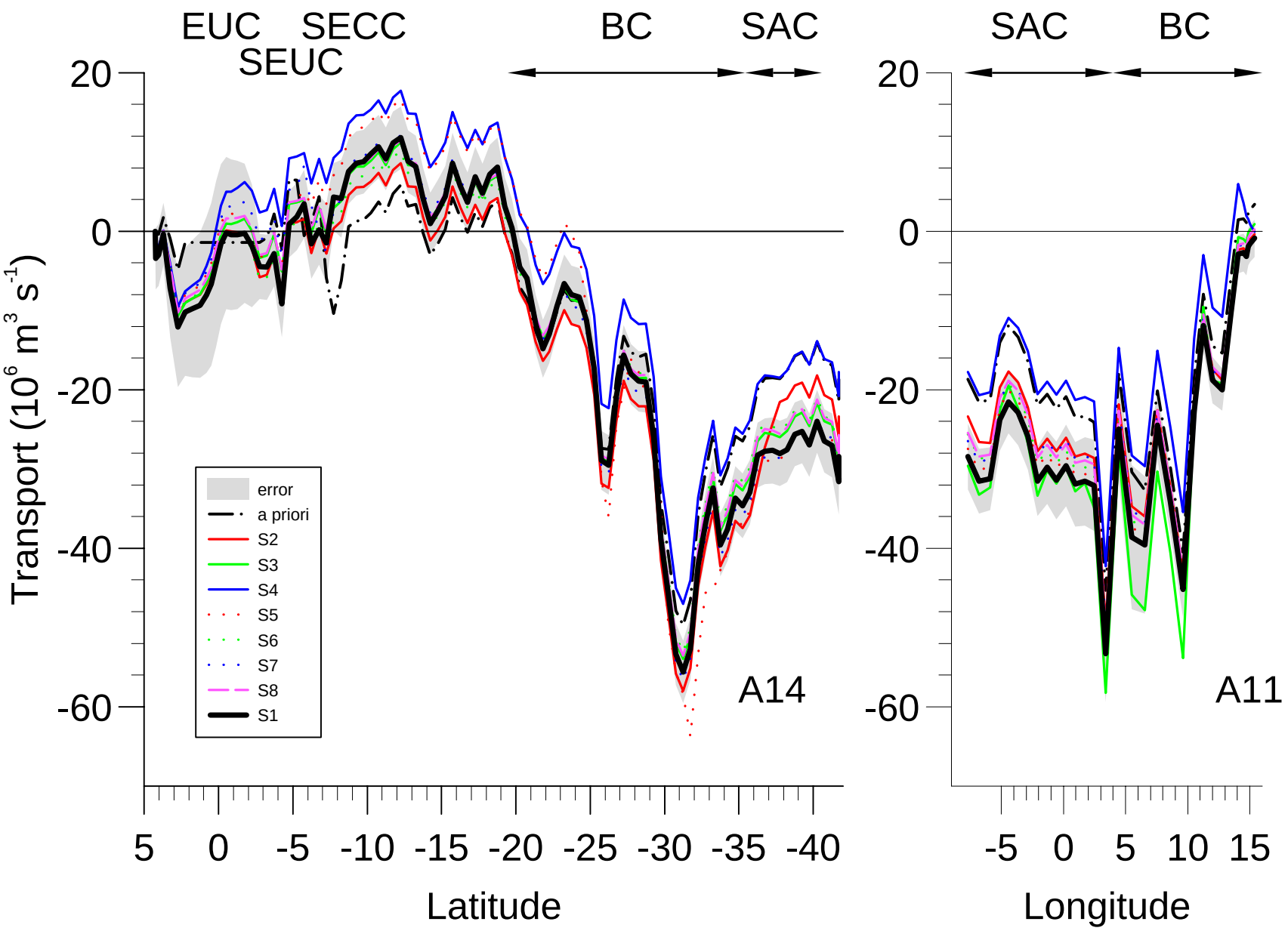
EUC
SECC
SEUC
BC
SAC
SAC
BC
20
0
-20
-40
-60
Transport (10^6 m^3 s^{-1})
error
a priori
S2
S3
S4
S5
S6
S7
S8
S1
A14
A11
5
0
-5
-10
-15
-20
-25
-30
-35
-40
-5
0
5
10
15
Latitude
Longitude

FIG 8

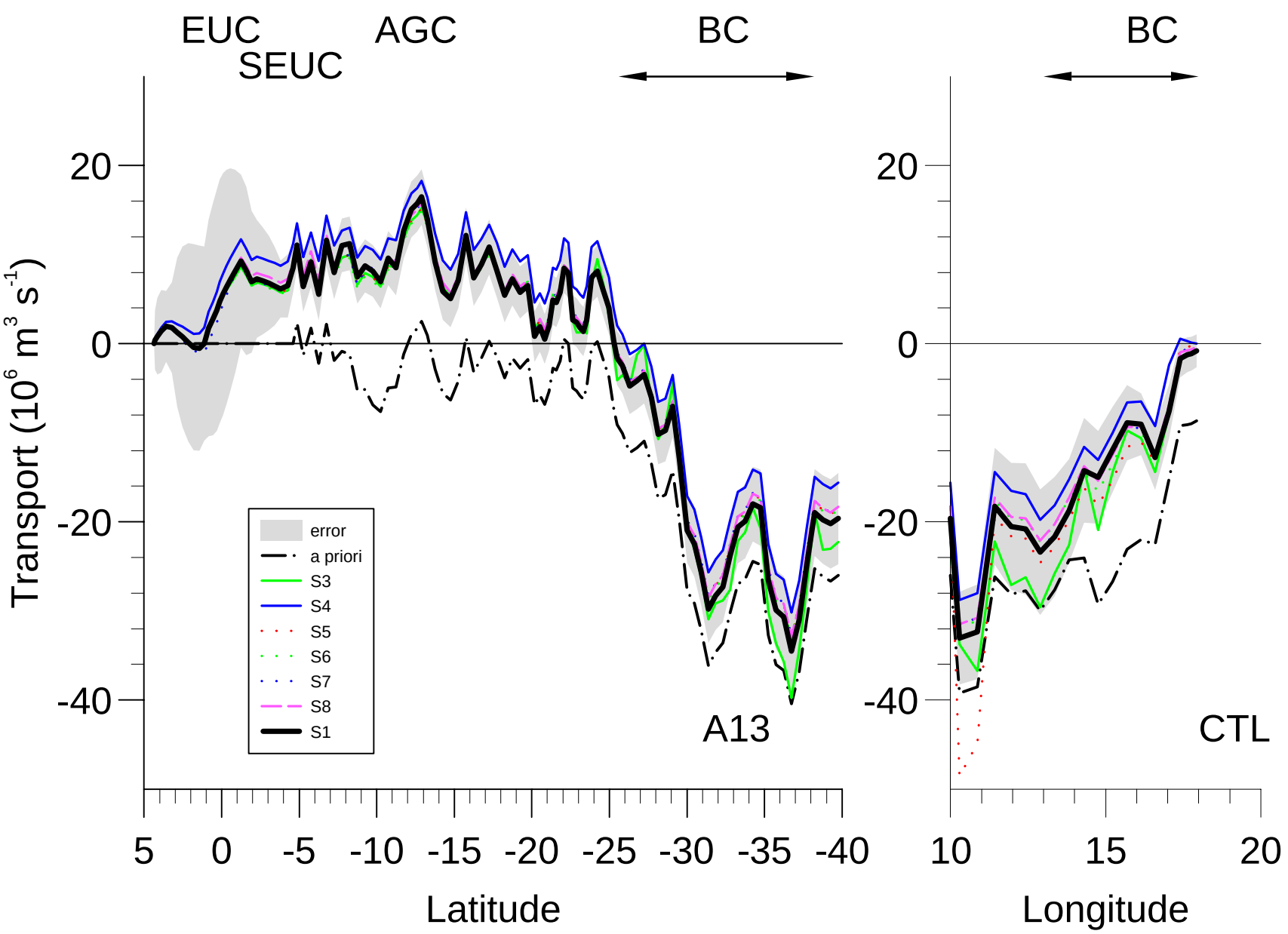
EUC
SEUC
AGC
BC
BC
20
0
-20
-40
Transport (10^6 m^3 s^{-1})
error
a priori
S3
S4
S5
S6
S7
S8
S1
A13
CTL
5
0
-5
-10
-15
-20
-25
-30
-35
-40
10
15
20
Latitude
Longitude

FIG9

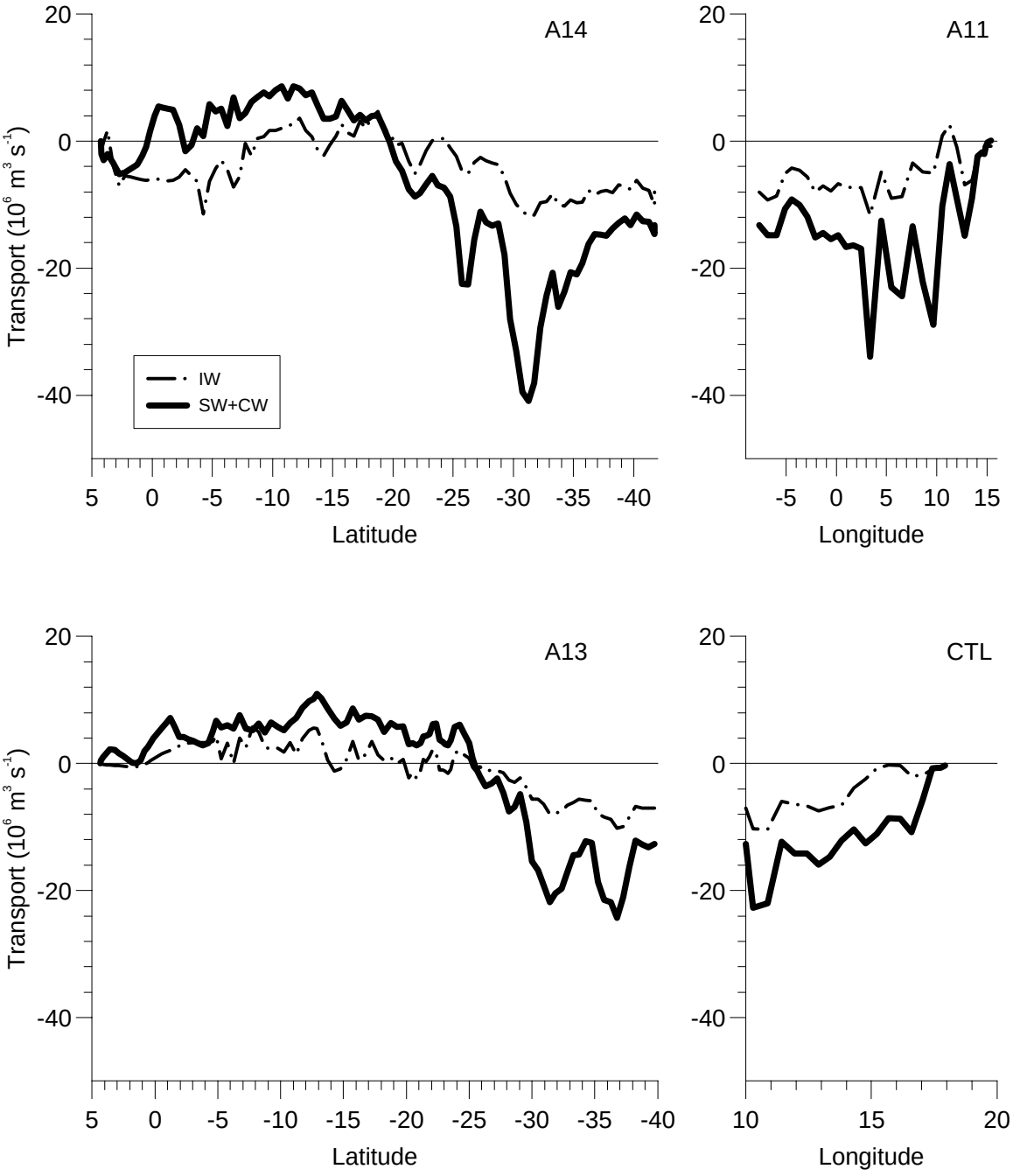
A14
A11
A13
CTL
IW
SW+CW
Transport (10^6 m^3 s^{-1})
Latitude
Longitude
20
0
-20
-40
5
0
-5
-10
-15
-20
-25
-30
-35
-40
10
15

FIG 10